Structure and molecular interactions in 1-ethyl-3-methylimidazolium bis(trifluoromethanesulfonyl) imide ionic liquid/carbonate co-solvents -– combined DFT and molecular dynamics study.

Abraham Molla Wagaye[1], Teketel Yohannes[3] and Getachew Adam Workneh[1]

[1]Addis Ababa Science and Technology University, P.O.Box 16417, Addis Ababa, Ethiopia.

[3]Ethiopian academy of science, P.O.Box Addis Ababa, Ethiopia

Corresponding Author :

Getachew.adam@aastu.edu.et/teketel.yohannes@aau.edu.et/abrhamollawagaye@gmail.com

Abstract

Both density functional theory (DFT) and molecular dynamics (MD) based on classical force field were used to provide both structural and electronic insight into the multifold interactions occurring in 1-ethyl-3-methylimidazolium bis(trifluoromethylsulfonyl)imide ionic liquid in the presence of ethylene carbonate and dimethyl carbonate co-solvent mixtures which are currently being targeted for applications in next-generation Li-ion battery electrolytes. In order to give a visual understanding of the molecular interactions, the structures of cations, anions, and cation - anion ion pairs were systematically studied using DFT calculations. The nature of hydrogen bond interactions in a series of ion pair conformers have been thoroughly discussed by analyzing the interaction energies, stabilization energies and natural orbital analysis of the ion pair conformers. Multiple but weak C−H---O/N hydrogen bonds and anion donor π^*_{C-N} interactions have been observed. Charge transfer occurs mainly from the lone pairs of oxygen and nitrogen atom to the σ-type anti-bonding orbital of the C–H bonds and π-type anti-bonding orbitals of N−C bonds. According to the MD study, the addition of carbonate co-solvents into the pure ionic liquid creates a more structured system than the pure ionic liquid. The coordination of the O/N atoms of the bis(trifluoromethylsulfonyl)imide anion to the most acidic H atom of 1-ethyl-3-methylimidazolium cation showed a marked decrease with increase in carbonate concentration indicating that the C− H---O/N hydrogen bond interaction is reduced by the presence of high carbonate content. Furthermore, in the pure ionic liquid, adjacent cations are almost exclusively located on top and below the ring cation, whereas the anions mainly coordinate to the cation within the ring plane. The addition of large amount of carbonate co-solvents disturb the original near ordering which is found in the pure ionic liquid.

Key words: electrolyte, Li-ion, 1-ethyl-3-methylimidazolium bis(trifluoromethylsulfonyl)imide, ethylene carbonate, dimethyl carbonate.

1 Introduction

Lithium-ion batteries (LIBs) are the main research interest for electrochemical and materials applications because of their excellent energy storage capability [1]. LIBS have good cycle life and can be manufactured in various forms that are better suited for a particular application [2]. Electrolytes are the key component of lithium ion battery that serve as a medium for transporting lithium (Li) ions between electrodes during the charge−discharge process [3]. Conventional electrolytes used in LIBs are usually composed of an organic solvent (e.g., ethylene carbonate, dimethyl carbonate and propylene carbonate) and Li salt (e.g., lithium hexafluorophosphate) [4]. These organic based electrolytes possess favorable features such as high ionic conductivities. However, carbonates are flammable which pose safety concerns and this limits their operative temperature range [5]. For these reasons, there have been a lot of research interests to develop alternative electrolytes that have improved safety and that would be able to work in a broader operative temperature range. Recently, a large number of alternative electrolytes have been suggested. Among them, ionic liquids (ILs) have been proposed as one of the solutions to the above safety concerns, mainly because of their high thermal and chemical stability, large electrochemical stability window, and their negligible vapor pressure [6]. The structural, [7] thermodynamic [8], and dynamic properties [9-10] of both pure ionic liquids and their mixtures with other compounds have been studied and documented by different authors that make use of both experimental and theoretical calculations.

Although ionic liquids possess desirable features as electrolyte components [11], further developments have been hindered by their high viscosity which induces low wettability of the electrode surface and low ionic conductivity. The most recent strategy employed to overcome this problem has been the use of electrolytes based on mixtures of ILs and organic electrolytes [12]. An appropriate selection of the type of ILs, solvent(s) and lithium salt, as well as the ratio between these components, makes possible the realization of electrolytes with optimized properties. For these reasons, the use of IL/carbonate mixtures has become a popular and a viable

strategy. Guerfi et al. [13] have investigated the electrochemical performance of mixtures containing 1-ethyl-3-methylimidazolium bis(trifluoromethanesulfonyl) imide [EMI][TFSI], ethylene carbonate (EC), diethyl carbonate (DEC) and $LiPF_6$ as lithium salt and found an optimum range of conductivity and viscosity for electrolytes containing 30–40% of ILs in the organic solvents. The electrochemical performance containing these mixtures was found to be comparable to that of conventional systems, with an extra advantage of improved safety. Wang et al. investigated the use of [EMI][TFSI] ILs in combination with propylene carbonate (PC), and found that these types of mixtures showed enhanced electrochemical features for use in LIBs [14]. More recently, Wilken et al. reported a detailed study about the influence of the amount of ILs on the viscosity, conductivity and flammability of mixtures containing [EMI][TFSI], EC, DEC, lithium bis(trifluoromethylsulfonyl)imide (LiTFSI) and lithium hexafluorophosphate ($LiPF_6$) lithium salts [15]. Furthermore, mixtures containing N-alkyl-N-methyl-pyrolidinium bis(trifluoromethanesulfonyl) imide [PYR][TFSI], PC and LiTFSI have also been investigated [16]. It has been shown that these mixtures have had enhanced conductivities, low viscosities, and overall stability windows of more than 5 V. A mixture containing 80 wt% ILs (flash point of 153°C) was found to be non-flammable with the extra advantage of reducing the kinetics of PC evaporation as well as the anodic dissolution of aluminum [16, 17].

Previous studies on blends of ionic liquids and organic carbonates paid particular emphasis on improved macroscopic properties such as safety performance and enhanced electro-chemical properties, while often neglecting the molecular details that govern the achievable ion transport properties of such blends, which are extensively considered in this work. Further studies on microstructures and interactions of ionic liquids at molecular level, as pure compounds or in the presence of dissolved species, is useful to design of suitable ionic liquids for a particular application, and this facilitates the selection of an optimum conditions of transport and thermodynamic properties. The ability to form mixtures of ILs with organic carbonates and other solvents has become increasingly important, and this is heavily influenced by the nature of those electrostatic interactions. Those properties are not accessible to experiments, yet important for boosting this innovative line of research by helping to and unravel all the fundamental microscopic features escaping experimental probes. The purpose of current work is, therefore, to unravel the microstructures and ion–ion interactions of ionic liquids at molecular level, both as pure components and in the presence of dissolved carbonate solvents and to critically compare

the impact of adding carbonate (EC/DMC) co-solvents on the ion–ion interactions and the structural properties of the corresponding blends using 1M LiTFSI as conducting lithium salt.

The $[TFSI]^-$ anion is of great interest for researchers as this anion forms hydrolytically stable ionic liquids with lower viscosity and high electrical conductivity [18]. Previous studies revealed that series of 1-alkyl-3-methylimidazolium and N-alkyl-N-methyl-pyrolidinium [TFSI] salts give ionic liquids at room temperature. Since then, the $[TFSI]^-$ anion was extensively studied as an anion of polymers [19] and electrochemical applications [20, 21]. The use of [EMI][TFSI] with relatively high ionic conductivity of 1.06×10^{-2} $S\cdot cm^{-1}$ and low viscosity at room temperature has already been reported for Li-ion cell [22, 23]. EC is the most widely used solvent in Li-ion batteries. It is solid at ambient conditions, for that reason, it is mixed with linear carbonates (di-ethyl, di-methyl, or ethyl-methyl carbonate: DEC, DMC, EMC) thus forming a liquid mixture with good polar characteristics. Equimolar mixtures of EC and DMC revealed better ionic conductivity (10.7 mS cm^{-1}) at room temperature compared to similar blends with LiTFSI (9.4 mS cm^{-1}) [24]. Therefore, it appears useful in our study to critically compare the impact of both a mixture of [EMI][TFSI], EC, DMC (EC/DMC: 50/50 wt%) and 1 M LiTFSI on the achievable molecular interactions of the corresponding IL/carbonate blends.

To date, molecular dynamics (MD) simulations in combination with experimental approaches have provided good insight into the structure and dynamics of ILs [25-28]. Quantum chemical methods are useful in developing and understanding, at the molecular level, the design of new and advanced ILs [29, 30]. This is because the molecular interactions between cations and anions, and the interplay between the short-range and long-range interactions, govern the details of ILs' physicochemical properties. The KohnSham (KS) density functional theory (DFT) is the most widely used method for electronic structure calculations in condensed matter physics and quantum chemistry. However, in general, the drawback of all the common functionals is their inability to describe long-range electron correlations responsible for noncovalent interactions [31, 32]. Coupled cluster theory with singles, doubles, and perturbatively connected triple excitations [CCSD(T)], in conjunction with large basis sets, can accurately describe these effects [33, 34]. Unfortunately, CCSD(T) calculations are computationally very demanding and therefore can be applied for systems with few atoms. Second-order Møller Plesset perturbation theory (MP2) [35] has a much lower computational cost, and is seen as a suitable method to

partly account for dispersive interactions in large systems. However, it tends to overestimate binding energies for π-stacked systems [36]. Due to the high cost of Coupled cluster methods, there has been considerable effort to capture the long-range correlation effects at a much reduced cost by nonempirical DFT based approaches [37] such as symmetry-adapted intermolecular perturbation theory (SAPT). However, since this representation of dispersion interactions is nonempirical in nature, the computational cost still represents a serious bottleneck. Therefore, the method of choice has been the use of DFT-D based description of non-covalent interactions, leading to several dispersion-corrected methods [38]. The simplest approach, normally designated as DFT-D, introduces dispersion interactions using an empirical potential [39]. The DFT-D has been applied to calculate the intermolecular interactions energies for large benchmark sets of noncovalent molecules with very satisfactory results [40]. The ωB97X-D functional has been shown to have the best performance in treating π-π intermolecular interactions and charge transfer excitations [41]. For large molecular systems where Coupled cluster is very expensive to use, the ωB97X-D functional can provide accurate description of intermolecular distances. Therefore, we believe that the ωB97X-D functional approach can also be an excellent alternative to deal with ionic liquids containing immidazolium based systems where the effect of dispersion interactions leads to ring stacking interactions and delicate intermolecular interactions like H-bonding occur predominantly.

Besides the functionals, the quality of the basis set is another important factor that affects the speed and accuracy of calculations. Since large basis sets, in general, yield more accurate results than smaller basis sets, triple-zeta basis sets or even larger have been routinely employed to compare different functionals. However, large basis sets make the calculations too slow for large systems. Smaller basis sets, such as those of double-zeta quality, could make the calculations faster but may not describe noncovalent interactions accurately, such as halogen bonding [42, 43]. Therefore, small basis sets, which could combine high computational speed and accuracy, are in great demand [44]. It has been shown that for halogen-bonded complexes for which the complexation energies have been previously calculated with more accurate CCSD(T)/CBS method, the DGDZVP basis set performed far better than other double-zeta basis sets, and it even outperformed the triple-zeta basis sets. Due to its small size, it is well suited for studying halogen bonding in large systems. The DGDZVP basis set in combination with ωB97XD functional has been shown to perform better than other double-zeta basis sets, and at least as

good as triple-zeta basis sets and is well-suited for calculating halogen bond strengths on large complexes [45]. The DGDZVP basis set has been used in our work in combination with ωB97XD functional and results were compared against previously reported experimental results as well as other basis sets such as 6-311++G(d,p), 6-311++G(3df,2dp). What is more, on account of higher accuracy, ab initio molecular dynamics (AIMD) simulations add valuable insight into solvation mechanisms and energetics of ionic salts in a variety of organic solvents, but they require relatively higher computational demands [46-48]. Due to the limited time- and size-scales of DFT methods and high cost of AIMD simulations, classical molecular dynamics (MD) has largely been the method of choice for investigations of IL structure [49-52]. Early imidazolium based ionic liquid force fields by the groups of Maginn [53, 54], Berne [55], and Stassen [56, 57] helped shape initial thoughts as to the origin of their unique solvent properties.

The purpose of the present article is to provide insights into the molecular and liquid structure of [EMI][TFSI] IL both in the pure state and in ternary mixtures using carbonate (EC/DMC) co-solvents, a potential electrolyte for next generation Li-ion battery. The article is structured as follows. First, we give a brief overview over the computational methods employed in this work. This is followed by the discussion of the structures of single cations, anions, and cation-anion ion-pairs of [EMI][TFSI] based ionic liquids. The interaction energies, stabilization energies and natural orbital analysis of the ion pair conformers are thoroughly analyzed and discussed. After this, the details of cation–cation, anion–anion, cation–anion and solvent–solvent interactions are studied by analyzing trajectories through the calculation of radial pair distribution functions (RDFs) [58], spatial distribution functions (SDFs) [59] and combined distribution functions.(CDFs) [60]. We mainly concentrate on the orientation of $[EMI]^+$ cations relative to each other as well as the coordination of $[TFSI]^-$ anions to the $[EMI]^+$ cations. Furthermore, we investigate the H-bond interaction between $[EMI]^+$ and $[TFSI]^-$, and how this behavior is influenced by the EC/DMC content.

2. Calculation Methods

2.1 DFT Calculations

DFT calculations have been carried out with the Gaussian 09 suite of programs [61]. Using the density functional theory with the hybrid B3LYP functional [62, 63] and with Grimme's B97D functional including dispersion [64]. All monomeric ion calculations at the B3LYP and ω97X-D levels have been carried out with the 6-311++G(d,p), 6-311++G(3df,2dp), and DGDZVD basis sets. All structures have been fully optimized both in the gas phase and using the polarizable continuum model (PCM) implemented in the Gaussian program. Electrostatic interactions of the ion pair with surrounding ions were effectively accounted for by introducing apparent dielectric constant ε for the RTIL environment. Previous reports show that this approach, originally introduced for quadrupolar solvents, such as benzene and supercritical carbon dioxide, was able to describe solvation effects in nondipolar solvents [65-66]. In the present study, we employed acetonitrile (ε = 36) to model [EMI][TFSI] in the PCM framework. The use of polarizable continuum model (PCM) is based on MD simulation results [67-69] that imidazolium-based ILs show somewhat larger solvatochromic shifts. Each structure has been individually optimized for each method. Natural bond orbital analysis (NBO) analyses for all the ILs was made at ω97X-D levelswith the DGDZVD basis set using the polarizable continuum model (PCM). This analysis helps us to identify specific orbital interactions, NBO charges and also to obtain the descriptions of orbital hybridization. Vibrational frequencies of all the optimized structures have also been calculated to ensure that the optimized structure represents the true minimum. The absence of imaginary vibrational frequency confirms that the optimized geometry represents the stable structure. Basis set superposition error (BSSE) correction was not employed as its contribution to the interaction energy for an ionic salt are already reported to be insignificant [70].

2.2 Molecular Dynamics Simulations

MD simulations were performed using LAMMPS (Large Scale Atomic/Molecular Massively Parallel Simulator) [71]. All potential models used to describe intermolecular interactions were based on the OPLS-AA force field (Optimized Potentials for Liquid Simulations/All Atom) [72]. In the non-polarizable OPLS-AA force field formalism, the total energy for each ionic liquid

system are evaluated as a sum of individual energies for the harmonic bond stretching and angle bending terms, a cosine series for torsional energetics, and Coulomb and 12-6 Lennard-Jones terms for the nonbonded interactions. Geometric combining rules for the Lennard-Jones coefficients were utilized. Nonbonded interactions were evaluated intermolecularly and for intramolecular atom pairs separated by three or more bonds. To apply the same parameters for both intra- and intermolecular interactions, the 1,4-intramolecular interactions were reduced by a factor of 2. A 12-6 Lennard-Jones (LJ) pair interaction model with 13.5 Å cut-off was used to model the van der Waal's interactions. The bonded and non-bonded parameters for EC and DMC were obtained from the OPLS-AA force fields [72-74], while those for $[EMI]^+$ and $[TFSI]^{- -}$ were taken from Lopes et al. [75] and Li^+ from Jensen et al. [76] Charges are downscaled to an absolute value of 0.8 to account for the charge transfer and polarizability within ILs.

The molecules were initially packed randomly in a cubic box using PACKMOL. [77] Compositions of the simulated ionic liquids are shown in **Table 1**. All simulation box consists of different fractions of 0-300 DMC, 0-300 EC, 86 Li^+, 86-356 $[TFSI]^-$ and 0-270 $[EMI]^+$ ions. Initial volume of the cubic box: 51.8 × 51.8 × 51.8 $Å^3$ is chosen such that the density of the system is closer to the reported density of [EMI][TFSI] (53.32 g/cm^3). Periodic boundary conditions were applied on all three sides of the cubic simulation box to represent the bulk solution. The system was simulated at temperature, T = 298 K and pressure, P = 1 atm. The velocity Verlet algorithm was used to integrate the equations of motion with a time step of 0.001 fs. The Nose´–Hoover thermostat and Berendsen coupling [78] barostat were employed to control the temperature and pressure of the system for the canonical ensemble (NVT) and isothermal–isobaric ensemble (NPT) ensemble. The Nose´–Hoover barostate and velocity rescaling with a stochastic term (v-rescale) were employed to control the temperature and pressure of the system during the microcanonical ensemble (NVE) ensemble [79]. The Ewald method was used for treating electrostatic interactions. The system was first energy minimized using conjugate gradient algorithm. Then, the system was equilibrated for 4 short runs of 150 ps each in the NVT ensemble, 14 short runs of 150 ps each in an NPT ensemble. Then, each system was further simulated for 10ns runs in the NVE ensemble. Finally, a 1ns trajectory was saved in the NPT ensemble for structural post trajectory analysis. The equilibration was assured by analyzing the system potential energy and relevant physicochemical properties such as density as a function of simulation time. The systems were visualized in VMD [80]. In order to explore the

structures of ion coordination geometries in the ionic liquid-carbonate mixtures relative to a central immidazolium cation ring $[EMI]^+$, we have generated radial distribution function (RDF), spatial distribution functions (SDFs), and combined distribution function using the TRAVIS software package [81] and built-in LAMMPS codes for calculations radial distribution function.

Table 1. The 4 investigated systems (IP refers to ion pairs of [EMI][TFSI]) using 1:1 EC/DMC wt/wt 1 M LiTFSI 298 K and 1 atm.

System	A	B	C	D
Composition	270IP	210IP 120 EC/DMC	150IP 300 EC/DMC	90IP 420 EC/DMC
Percentage wt/wt	100 IP	63.63 IP 36.37 EC/DMC	33.33 IP 66.67 EC/DMC	17.65 IP 82.35 EC/DMC
Density [g/cm^{-1}]	1.631705	1.471591	1.378376	1.218262

3. Result and Discussion

3.1 Geometric Analysis

3.1.1 Single Ions

In order to give a visual understanding of the cation–anion interaction before designing initial geometries for the ion pairs (dimers), the most stable geometries of the isolated $[EMI]^+$ cation, and $[TFSI]^-$ anion conformers were revised and analyzed first. The atomic numbering scheme employed in the present work is displayed in **Figure 1**. The geometries of both $[EMI]^+$ cation and $[TFSI]^-$ anion were optimized directly at the B3LYP/6-311++G(d,p), B3LYP/6-311++G(3df,2dp), B3LYP/DGDZVP, ω97X-D/6-311++G(d,p), ω97X-D/6-311++G(3df,2dp) and ω97X-D/DGDZVP level both in gas phase and the presence of polarizable dielectric continuum medium using acetonitrile as a solvent. Vibrational frequencies of all the optimized structures have also been calculated to ensure that the optimized structure represents the true minimum. The absence of imaginary vibrational frequency confirms that the optimized geometry represents the stable structure. The structures of the fully optimized $[TFSI]^-$ anion and $[EMI]^+$

cation, respectively, are shown in **Figure. 2** and **Figure 3**. Selected structural parameters for $[EMI]^+$ cation and $[TFSI]^-$ anion are compiled in **Tables S1-S6**.

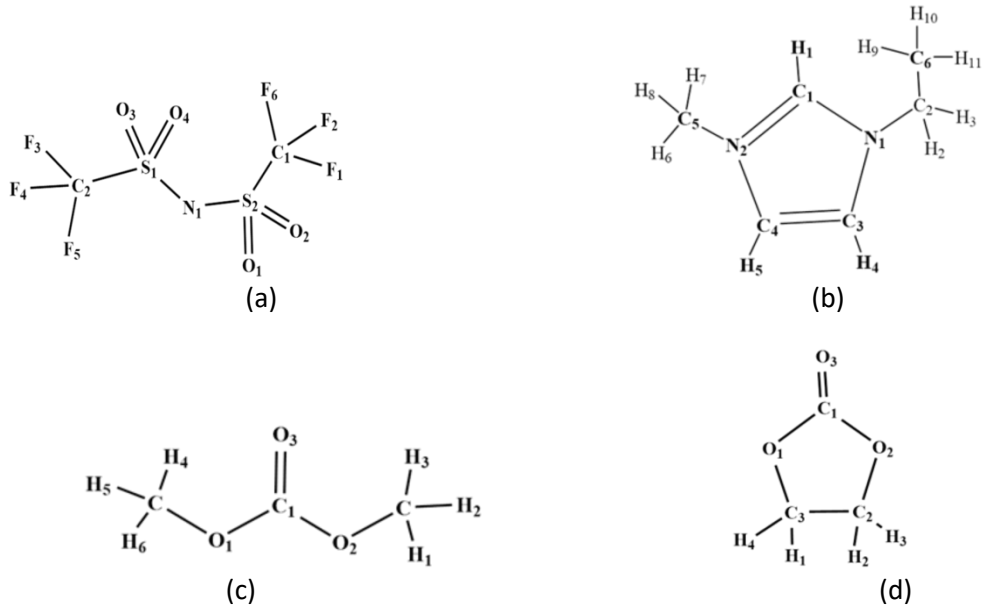

Figure 1: The atomic numbering scheme employed in the present work (a) $[TFSI]^-$ (b) $[EMI]^+$ (c) DMC (d) EC

The results of our calculated structural parameters of the cis and trans conformers of $[TFSI]^-$ anion are compiled in **Tables S1-S3**. Similar to previously reported results [82-89], we obtained two optimized minimum energy structures without imaginary frequencies. According to our results, the $[TFSI]^-$ anion exists in two different conformations: one with trans-symmetry where the CF_3 group are on opposite sides of the C-S-N-S dihedral angle, and another with cis-symmetry where the CF_3 groups are on the same side of the C-S-N-S dihedral (see **Figure 2**). On the basis of ωB97X-D/6-311++G(3df,2dp) functional and in the presence polarizable dielectric continuum medium (**Table S2** and **S4**) , we found that the conformers with the C-S-N-S dihedral angles 95.35°, 95.35° (trans-$[TFSI]^-$) and 87.6716, -128.195) (cis-$[TFSI]^-$) give the global and local minima, respectively, with the SCF energy difference of 3.025 kJ mol^{-1}**.** Our results show slight difference to previous results by Takamuku and coworkers where on the basis of B3LYP/6-311+G(d) calculations [89, 90], the values of the dihedral angles were (90.9°, 90.9°) for the trans geometry and (-81.2°, 120.2°) for the cis geometry, with the SCF energy difference of 2.3 kJ mol^{-1}. The deviations of the dihedral angles for B3LYP calculations

compared to our results on the basis of the ωB97X-D functional stems from the description of dispersion forces for which B3LYP density functional fails [91].

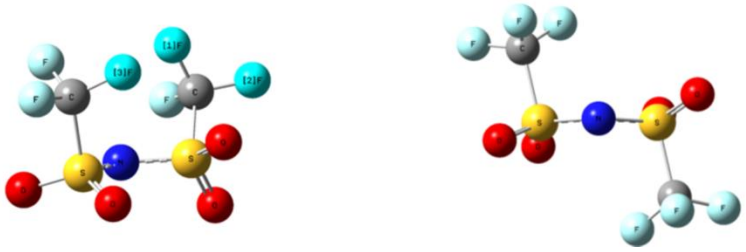

(a) cis (b) trans

Figure 2: Gas phase structures of (a) cis and (b) trans conformers of $[TFSI]^-$) optimized at ω97XD/6-311++(3df,2dp).

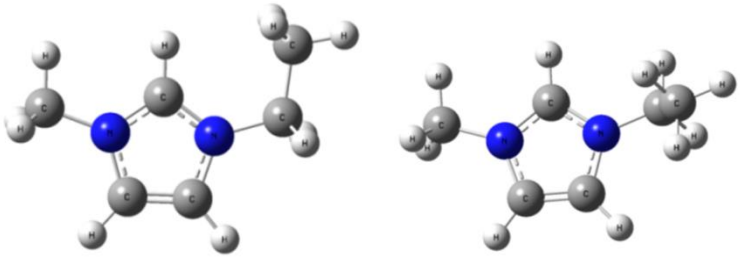

(a) planar cis (b) non-planar staggered

Figure 3: Gas phase structures of (a) planar and (b) nonplanar conformers of EMI optimized at ω97X-D/6-311++(3df,2dp).

As can be seen from **Tables S1-S4**, bond lengths, angles and dihedrals of the conformers calculated using the ω97X-D level of theory are in good agreement among the various basis sets and the ω97X-D/6-311++(3df,2dp) level of theory and basis set gives calculated results that best agree with those in crystals [89]. On the other hand, bond lengths calculated using the B3LYP level of theory show some variations larger than those in the crystals [93] as well as than that of ω97X-D results. These imply that the wB97X-D functional with a larger basis set with polarization functions show good performance for such molecules involving fluorine or sulfur atoms [94]. The energy of the cis-$[TFSI]^-$ conformer relative to that of the trans-$[TFSI]^-$ conformer calculated using ω97X-D/6-311++(3df,2dp) levels of theory and the basis set and in the presence of dielectric continuum medium employed here is 3.025 kJ mol^{-1}. The small value, relative to the RT value at 298 K implies that the conformers are present in equilibrium. The dipole moment of the conformers is also shown. According to the ω97X-D/6-311++(3df,2dp) levels of theory and basis set and in the presence of dielectric continuum medium, the dipole

moment of the cis-$[TFSI]^-$ (μ = 6.0640) conformer is significantly larger than that of the trans-$[TFSI]^-$ (μ = 0.1107) one, implying that the cis-$[TFSI]^-$ geometry is preferred around small sized cations.

In our study, the geometries of the $[EMI]^+$ cation was optimized directly at the B3LYP/6-311++G(d,p), B3LYP/6-311++G(3df,2dp), B3LYP/DGDZVP, ω97X-D/6-311++G(d,p), ω97X-D/6-311++G(3df,2dp) and ω97X-D/DGDZVP level both in gas phase and the presence of polarizable dielectric continuum medium using acetonitrile as a solvent. Selected structural parameters of the planar-cis and non-planar staggered conformers are compiled in **Tables 6-9**. The optimized geometrical structures of $[EMI]^+$ cation are shown in **Figure 3**. According to our results, the most stable geometry ω97X-D/6-311++G(3df,2dp) level of theory showed a non-planar staggered with the dihedral angles N_7-C_5-N_8-C_{13} and C_9-N_7-C_5-H_6 of 177.684° and 0.334° respectively (**Table 9**). Our results show agreement with previously reported results [95-99].

As can be seen from **Tables S5-S8**, bond lengths, angles and dihedrals of the conformers calculated using the ω97X-D level of theory are in good agreement among the various basis sets and the ω97X-D/6-311++(3df,2p) level of theory and basis set, and gives calculated results that best agree with those in the crystals [100-103]. On the other hand, bond lengths calculated using the B3LYP level of theory show some variations larger than those in the crystals1[100-103] as well as ω97X-D. The energy of the planar-cis $[EMI]^+$ conformer relative to that of the non-planar staggered $[EMI]^+$ conformer calculated using the ω97X-D/6-311++(3df,2p) levels of theory and basis set and in the presence of dielectric continuum medium is 9.8 kJ mol^{-1}. According to the ω97X-D/6-311++(3df,2p) levels of theory and basis set and in the presence of dielectric continuum medium, the dipole moment of the non-planar staggered $[EMI]^+$ (μ =2.0550) conformer is slightly larger than that of the planar-cis $[EMI]^+$ one (μ = 1.3131), implying that the non-planar staggered $[EMI]^+$ geometry is preferred around more small sized anions.

3.1.2 [EMI][TFSI] Ion Pair Conformers.

After analyzing the influence of the level of theory and basis sets for the monomeric ions, to further investigate the molecular interactions and conformational states of 1-ethyl-3

methylimidazolium bis(trifluoromethylsulfonyl)imide ion-pairs ([EMI][TFSI]), geometry optimization of each ion pair conformer was done on isolated ion pair with ωB97X-D/DGDZVP level of theory and basis set. Electrostatic interactions of the ion pair with surrounding ions were effectively accounted for by introducing apparent dielectric constant (acetonitrile) for the RTIL environment. To avoid the effect of change of basis sets, all calculations are performed using the same basis set. Concentrating now on the ωB97x-D/ DGDZVP results only, the intra- and interionic bond lengths, angles, dihedral angle in different ion pair conformations are compiled in **Table 2**. For convenience, the atomic numbering scheme employed in the present work is displayed in **Figure 1**. There are five different minimum energy different conformations available for [EMI][TFSI] ion pair that could be connected via the most acidic proton (H_1) of the cation or via the other protons of the methyl and ethyl group hydrogen's of the cation (see **Figure 4** and **5**). Vibrational frequencies of all the optimized structures have also been calculated to ensure that the optimized structure represents the true minimum. The absence of imaginary vibrational frequency confirms that the optimized geometry represents the stable structure. The optimized geometrical structures of cation-anion pairs are shown in **Figure 4**.

Previous studies by Umebayashi et al. [103] on the molecular conformations of [EMI][TFSI] by Raman and infrared spectroscopy showed that the $[TFSI]^-$ anion in the trans conformation was favored over the cis-$[TFSI]^-$ anion. The temperature dependence of its conformational changes has also been examined experimentally by Lassegues et al. [105]` and Koddermann et al. [106] Tsuzuki et al [107]. have noted in their ab initio study that the magnitude and directionality of ion pair interactions are important to the dissociation and association behaviors of the ions in RTILs. The most recent studies on the conformational states of [EMI][TFSI] were performed via the ab initio methods at the density functional theory (DFT) and via experimental Raman and FT-IR spectroscopy [108, 109]. In those studies, the different conformers of the [EMI][TFSI] cation−anion pairs were optimized at B3LYP level in the gas phase and in a dielectric continuum solvent environment, and found that the anion in the lowest energy ion pair state adopted a trans conformation. Those studies showed that, in the gas phase, the lowest energy conformer exhibited a characteristically strong $C_1{-}H_1{---}N_1$ interaction through the $C_1{-}H_1$ cation bond, accompanied by a substantial red shift of $C_1{-}H_1$ stretching vibrational frequency. However, those studies reported so far have focused only on the conformational preferences of the $[TFSI]^-$ anion (as either cis-$[TFSI]^-$ and/or trans-$[TFSI]^-$) while no indications were made on the

conformational preference of the $[EMI]^+$ cation (as either non-planar staggered $[EMI]^+$ and/or planar cis $[EMI]^+$). The B3LYP functional fails to represent dispersion interaction (i.e, optimized structure may result in saddle point instead of global minimum), and thus the hybrid functional B3LYP offers poor description of the electronic structure of [EMI][TFSI] and is clearly inferior to ωB97X -D functional [110] which has not been given due consideration by those studies mentioned above.

Table 2: Bond distance, bond angle and dihedral angles of between $[EMI]^+$ cation and $[TFSI]^-$ anion in dielectric continuum using ωB97x-D/ DGDZVP level of theory and basis set.

Acceptor – Donor	**C_1**	**C_2**	**C_3**	**C_4**	**C_5**
Bond length (Å)					
C_1-H_1	1.07889	1.07817	1.07804	1.07719	1.08153
C_1-H_1--O_1	2.33307	2.40054	2.79484	2.51111	2.1758636
C_5-H_8--O_1	2.56533	2.55313	2.76501	2.42109	2.42161
N_2-C_1--O_1	3.18767	3.11698	3.12324	3.30809	3.1294
C_1-H_1--O_3	4.17733	4.15421	3.51671	4.15906	2.38871
C_2-H_2--O_3	2.79919	3.16777	2.41806	2.57019	2.63206
N_1-C_1--O_3	3.90883	3.65739	4.18176	4.02111	3.058
C_5-H_8--F_1	5.52536	5.12595	3.79813	5.02815	2.88651
C_6-H_9--F_3	2.83018	4.7277	2.72126	2.73334	2.82859
C_2-H_2--N_1	3.83064	2.75629	2.9609	3.68491	5.07138
C_1-H_1--N_1	2.80760	2.84439	2.63625	2.61455	3.78727
N_1-C_1--N_1	3.09642	3.02117	3.12034	2.96703	4.65852
C_6-H_9--N_1	2.58145	4.98124	2.6368	2.55063	5.06497
Bond angle (Deg)					
<C1-H1---O1	134.90792	122.62125	97.45009	130.00118	145.72274
<C5-H8---O1	140.08964	137.23789	97.2522	149.85344	150.0253
<N2-C1----O1	100.90634	98.4673	83.65041	96.71181	102.342
<C1-H1---O3	57.51002	55.73556	121.46364	75.20051	118.62975
<C2-H2---O3	113.78501	83.05732	145.26464	127.16128	114.59376
<N1-C1----O3	65.23194	55.05644	81.4531	64.01165	94.71732
<C6-H9----F3	142.77348	97.68907	120.32157	138.0436	155.72293
<C5-H8----F1	110.99608	127.13314	101.21089	99.26465	89.56325
<C1-H1---N1	95.12519	88.82750	106.60753	98.23770	139.06389
<N1-C1----N1	100.57534	89.37235	93.76557	101.11009	125.30961
<C6-H9----N1	147.94347	75.4204	130.27446	144.1511	135.42838
<C2-H2---N1	84.28362	121.46653	106.40545	85.42306	121.53507
Dihedral angle (Deg)					
<N1–C1–H1–O1	132.13557	122.07674	121.19799	135.73071	171.15364

<N1–C1–H1–N1	84.17610	74.07735	65.45483	81.88531	100.77334
Dipolment (μ)	20.351	15.4135	18.7817	17.6402	20.351
E (Hartree)	-2171.66729881	-2171.66686501	-2171.66857647	-2171.66883410	-2171.66748825

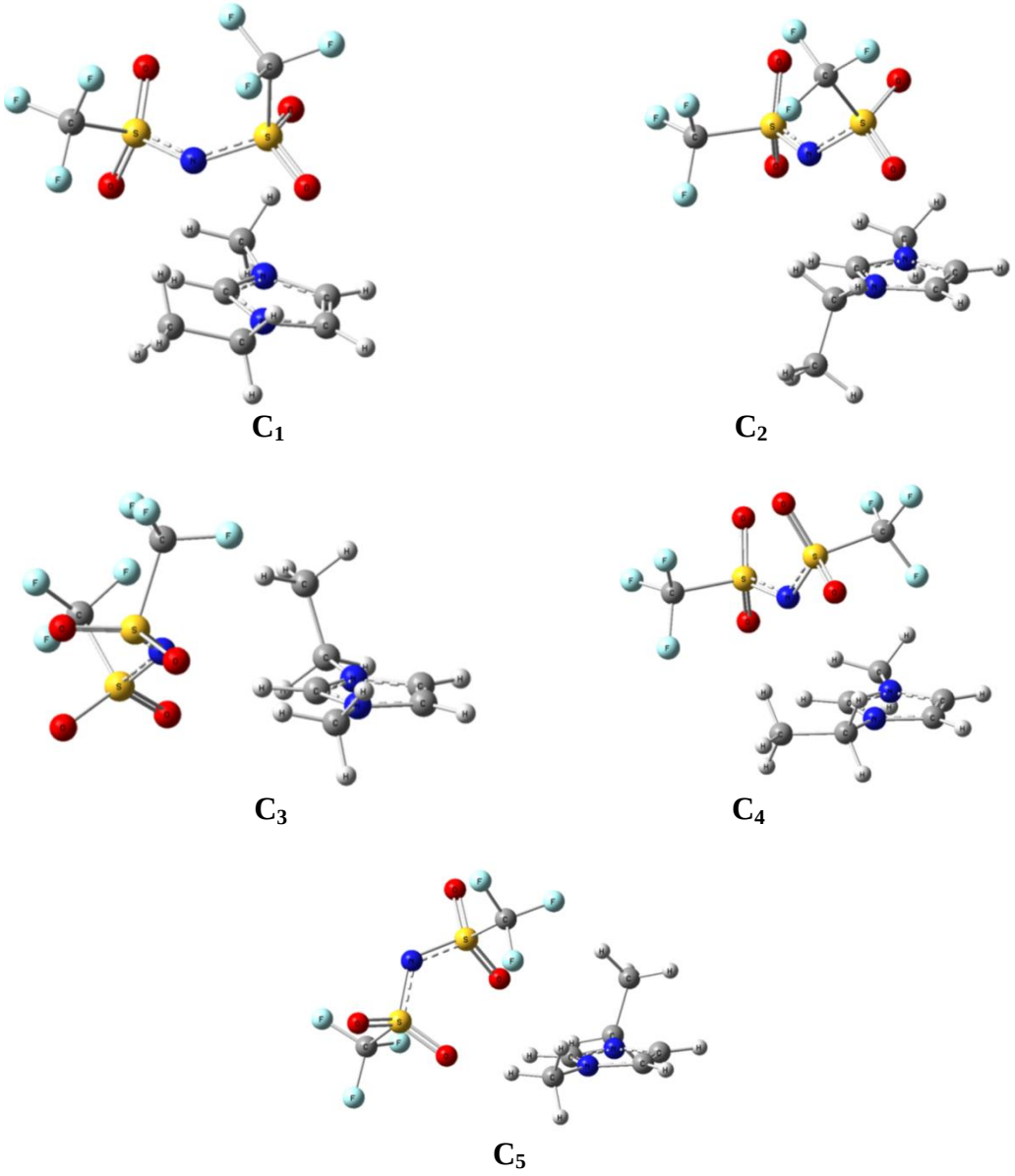

Figure 4: The optimized geometrical structures of cation-anion pairs in dielectric continuum medium using ωB97x-D/DGDZVP level of theory and basis set. C_1(Planar cis[EMI]---cis [TFSI]), C_2 (Staggered nonplanar[EMI]---cis [TFSI]), C_3(Staggered nonplanar[EMI]---cis [TFSI]), C_4 (Planar cis[EMI]---trans [TFSI]), C_5(Staggered nonplanar[EMI]---trans [TFSI]).

The present work, therefore, focuses on the molecular interactions and conformational analysis of [EMI][TFSI], by making use of detailed NBO analysis and multiple interaction sites (in addition to the C_1-H_1—N_1 and C_1-H_1---O_1 interactions) and the conformational preferences of the cation as either non-planar staggered and/or planar cis $[EMI]^+$ cation. In our study, all possible combinations of planar cis $[EMI]^+$ - cis $[TFSI]^-$, planar cis $[EMI]^+$ - trans $[TFSI]^-$, non-planar staggered $[EMI]^+$ - cis $[TFSI]^-$ and non-planar staggered $[EMI]^+$ - trans $[TFSI]^-$ were analyzed using wB97X-D/DGDZVP functional and basis set. As presented in **Table 2** and **Figure 4**, a total of five minimum energy different stable ion pair conformers (C_1–C_5) were obtained. The energetic difference relative to the lowest energy ion pair conformer ranges from 0.676 to 5.170 kJ/mol. The selected optimized structural parameters of the stable conformers, C_1-C_5, are shown in **Table 2**. The stability of the conformers depends on the number of molecular interactions as well as their strength and the mutual orientation between the cation and anion [111]. According to our results, the C_4 (**Figure 4**) ion pair conformer was found to be the lowest energy conformer. From our closer inspection of the C_4 ion pair conformer, we found that the C_4 ion pair conformer constitutes the planar cis $[EMI]^+$ - trans $[TFSI]^-$ ion pair configuration with the $[TFSI]^-$ anion on top position. The second, third, fourth and fifth lowest energy conformations predicted were, respectively, non-planar staggered $[EMI]^+$ - cis $[TFSI]^-$-syn (C_3), planar cis $[EMI]^+$ - cis $[TFSI]^-$ (C_1), non-planar staggered $[EMI]^+$ - trans $[TFSI]^-$ (C_5) and non-planar staggered $[EMI]^+$ - cis $[TFSI]^-$ -anti conformers (C_2), respectively. The $[TFSI]^-$ anion in the C_4 and C_5 states was found to adopt a trans conformation for the C−S−S−C dihedral angle, whereas a cis conformation was predicted for C_1, C_2 and C_3 ion pair conformers. The values of the dihedral angles N_1–C_1–H_1–O_1 for the ion pair conformers of C_1, C_2, C_3 and C_4, respectively, are 132.14°, 122.08° and 135.73° indicating that the $[TFSI]^-$ anion is on top position with respect to the imidazolium rings. On the other hand, the value of the dihedral angle N_1–C_1–H_1–O_1 for the C_5 ion pair conformer is 171.15° indicating that the $[TFSI]^-$ anion is nearly coplanar with the imidazolium rings.

The study of H-bonds in ILs is multifaceted with a range of experimental and computational methods employed. A traditional H-bond involves complex intermolecular interactions represented by X–H----Y, where a H-atom intercedes between two electronegative species X and Y, such as O or N. Standard H-bonds are primarily electrostatic interactions with covalent and dispersion contributions [112]. The concept of X–H----Y hydrogen bonds may be extended to

ionic liquids. Nevertheless, the characteristics and features of H-bonding in ILs cover an extremely wide and diverse range which is still the subject of scientific debate, and are thus not fully understood. H-bonding is not a binary on–off phenomenon but occurs in a graduated scale which makes quantifying and clearly demarking H-bonding difficult. To differentiate the H-bond in IL from other ionic H-bonds, we refer to the H-bond between $[EMI]^+$ and $[TFSI]^-$ species as the doubly ionic H-bond. Doubly ionic H-bonds are very common and occur within a large range of ILs. There are best reviews available in this topic [113]. The doubly ionic H-bond between $[EMI]^+$ and $[TFSI]^-$ species is bifurcated, and unlike many molecular liquids, a significant variety of distinct H-bonds are formed between different types and numbers of donor and acceptor sites within the $[EMI]^+[TFSI]^-$ ion pair (see **Figure 5** and **6**). Aprotic imidazolium based ILs typically exhibit weak H-bonds. However, Large anions such as the $[TFSI]^-$ anion typically have multiple H-bonding interaction sites within different ion pair conformers, increasing the overall energy contribution from H-bonds and π-type interactions [113].

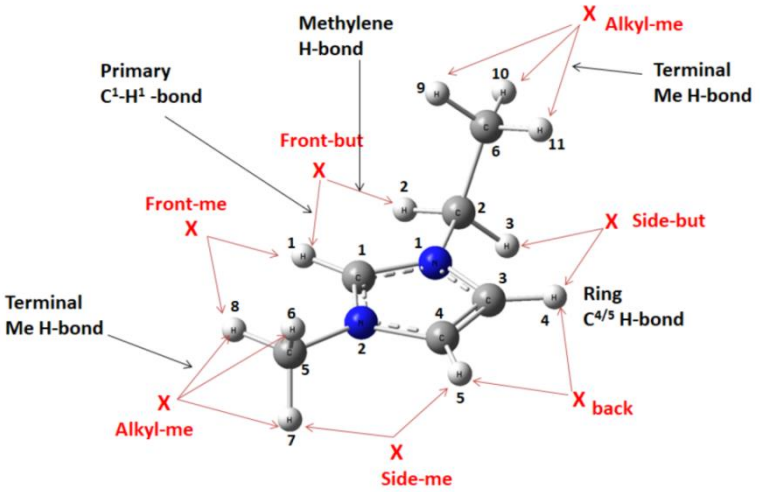

Figure 5: $[EMI]^+$ cation showing the possible interaction sites for the $[TFSI]^-$ anion (represented as X); anticlockwise these are front-me, alkyl-me, side-me, back, side-but, alkyl-me and front-but.

Following the recommendations and naming conventions of Patricia [113, 114] and coworkers, the possible interaction sites of the $[EMI]^+$ cation with the $[TFSI]^-$ anion are indicated in **Figure 5**. As shown in **Figure 5**, there are different association sites for the $[TFSI]^-$ anion within the $[EMI]^+$ cation: front-me, front-but and alkyl-me positions. The C_1, C_2 and C_5 ion pair conformers have front-me, front-but and terminal methyl H-bond interactions. The C_3 and C_4 ion pair conformers, on the other hand, exhibit front-me, front-but, methylene and terminal methyl H-

bond interactions. The ion pairs in C_1, C_3 and C_4 conformations exhibit bifurcated C−H---N_1 inter ion interactions through the primary C_1−H_1 and terminal methyl C_6−H_9 cation H-bonds. The ion pairs in C_1, C_2, C_4 and C_5 conformations exhibit bifurcated C−H---O_1 inter ion interactions through the primary C_1−H_1 and terminal methyl group C_5−H_8 cation H-bonds (see **Figure 6**). In addition to the primary front-me C−H---O_1 inter ion interactions, there also exist a secondary front-but C−H---O_3 inter ionic interactions for C_3, C_4 and C_5 ion pair conformers through the methylene group C_2−H_2 cation bond. Very weak C−H---F interactions have also been observed for all conformers except for the C_2 ion pair conformer through terminal methyl C_5−H_8 and C_6−H_9 cation H-bonds.

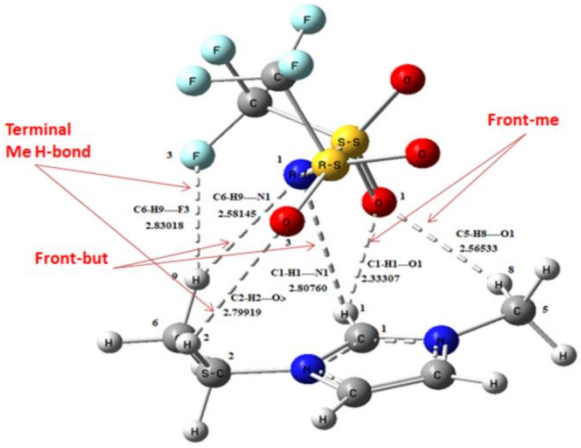

C_1

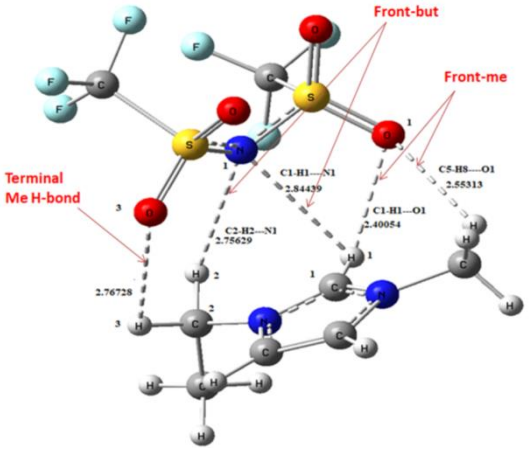

C_2

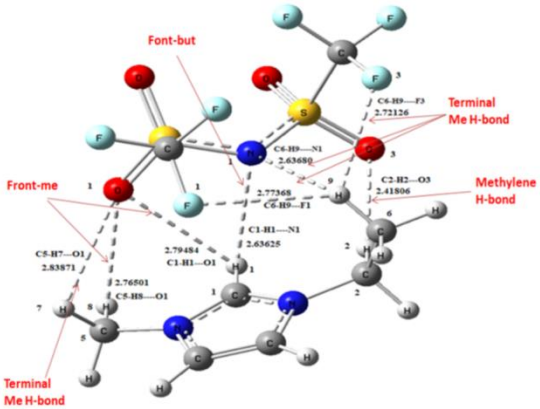

C_3

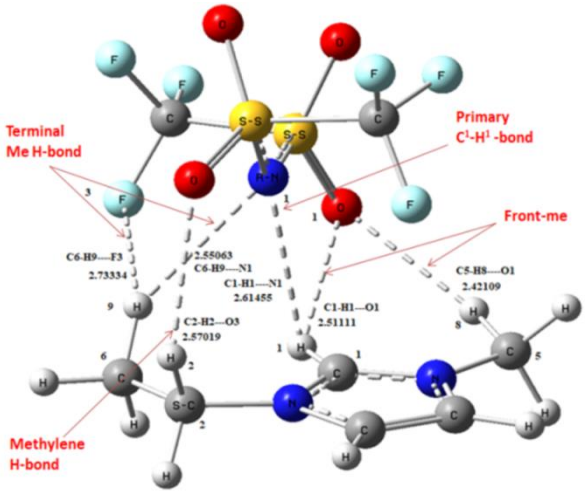

C_4

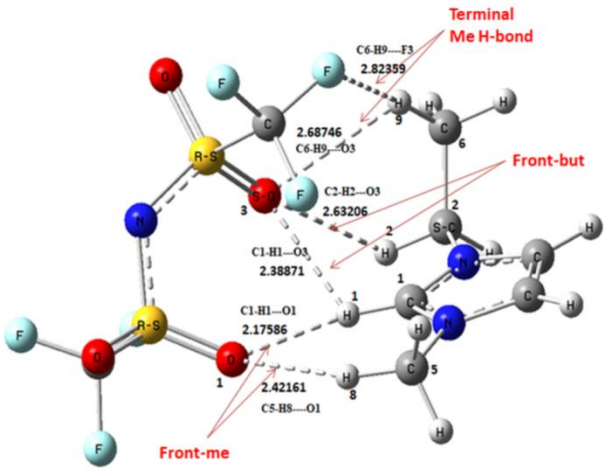

C_5

Figure 6: Different interaction patterns between the $[EMI]^+$ cation ring and $[TFSI]^-$ anion at ωB97x-D/ DGDZVP level of theory and basis set and in the presence of dielectric continuum medium. The $[TFSI]^-$ anion occupying multiple "sites" (front-me, front-but, terminal Me H-bond) around the $EMI]^+$ cation ring forming bifurcated H-bonds are indicated.

The values of the distances of $C_l–H_1---O_1$ for the ion pair conformers C_1, C_2, C_4 and C_5, respectively, are 2.30Å, 2.45Å, 2.51Å and 2.18Å which are shorter than the sum of the corresponding van der Waals radii for H (1.20Å) and O (1.52Å); and the corresponding respective values for angles for $C_l–H_1---O_1$ are 134.91°, 122.62°, 130.00° and 145.73°, which are within the accepted criteria of the $C_1–H_1---O_l$ H-bonds, which implies that the $[TFSI]^-$ anion forms H-bonds with $C_l–H_1---O_1$ and $Cl–H_1---N_1$ fragments of the $[EMI]^+$ ring cation (see **Table 2**). The type, number and strength of the different cation–anion molecular interactions play a crucial role in the overall conformer stability. According to Gilli et al. [111], it is possible to relate the strength of the H-bond (and hence the stability of conformers) to the donor-acceptor distance as a first estimate. The stability of C_4 ion pair conformer can be attributed to the favorable orientations of the O and N atoms in $[TFSI]^-$ anion towards the proton-donating groups of the terminal methyl and methylene hydrogen atoms of the $[EMI]^+$ cation. In the C_4 conformer, there exist bifurcated hydrogen bond interactions through primary front-me $C_1–H_1---O_1$ (with a distance 2.50 Å and an angle of 130.00°), front-me $C_5–H_8---O_1$ (with a distance 2.42 Å and an angle of 149.80°) and through the terminal methyl group hydrogen atoms of $C_6–H_9---N_1$ (with a distance 2.55Å and an angle of 144.15°) cation bond (see **Figure 6**). Thus, by relating the strength of the H-bond (and thus the stability of the conformer) to the donor-acceptor distance as

a first estimate, there are multiple shorter and more linear hydrogen bonding interaction sites in the C_4 ion pair conformer and hence is more stable than the least stable C_2 ion pair conformer by 5.17 kJ mol^{-1}. In the least stable ion pair conformer (C_2), the terminal methyl group hydrogens are in the anti-position with respect to the position of the O and N atoms of the $[TFSI]^-$ anion in the imidazolium ring, and thus the approaching oxygen (C_2–H_2---O_3) and nitrogen atoms (C_6–H_9---N_1) cannot make favorable H-bonding interactions to the terminal group hydrogen atoms of the cation and thus making it the least stable of all other conformers. The distance between the hydrogen atom at the C_1 position of the cation and the hydrogen bond acceptor atom of the anion for primary C_1–H_1---O_1 interaction is shorter for conformers C_1, C_2, C_4 and C_5 than similar distances for C_1–H_1---N_1 and C_1–H_1---F interactions (see **Table 2**). This suggests that the interionic H-bond interaction of the former is stronger than the latter two. When imidazolium cations are associated with large anionic groups, like $[TFSI]^-$ anion [114-117]**,** there exist multiple H-bond interaction sites within the liquid environment and exhibit varying levels of H-bond strength and directionality. Additionally, these large anions take preferential on-top distributions above and below imidazolium rings, leading to π-type interactions. The delicate interplay of H-bond and π-type interactions in [EMI][TFSI] ionic species becomes more complicated than this and requires further investigation.

3.2 Interaction Energies In [EMI][TFSI] Ion Pair Conformers.

The local nano-structural organization and physicochemical properties of ILs arise as a direct consequence of the characteristics of the constituent ions and the intermolecular interactions present between the ions in individual systems [118]. ILs are dominated by columbic and weak intermolecular interactions that gives rise to the unique physical and chemical environment present in each IL. Aiming at investigating the molecular interactions and the occurrence of H-bonding in [EMI][TFSI] ion pairs, the interaction energy of the different ion pair conformations were calculated using ωB97x-D/ DGDZVP level of theory and basis set and the results are shown in **Figure 7**. The interaction energy between the cation and the anion of the ILs was calculated according to the following expression:

$$\mathrm{E}\left(\frac{\mathrm{kJ}}{\mathrm{mol}}\right) = \mathrm{E(IP)} - (\mathrm{E(cation)} + \mathrm{E(anion)})$$

Where E(IP) is the energy of the ion pair, and E(cation) and E(anion) are the energy of the cation and anion, respectively. For the ion pair [EMI][TFSI], the absolute value of the interaction energies is lower than the normal hydrogen bond energies (50 $KJ.mol^{-1}$), which indicates that there exist strong electrostatic attractions between the imidazolium cations and TFSI anions.

The correlations between interaction and relative conformer energies of the different [EMI][TFSI] conformers are shown in **Figure 7**. The C_4 ion pair conformer has the maximum and C_2 and C_5 conformers have the minimum absolute interaction energies. Comparison between between interaction and relative conformer energies reveals that there are very important variations between the ordering of calculated relative and interaction energy values. According to **Figure 7**, the relative stabilities among the five conformers changes in the following order: $C_4 > C_3 > C_5 > C_1 > C_2$ whereas the absolute interaction energies change in the order: $C_4 > C_1 > C_3 > C_2 > C_5$. The absolute values of the interaction energies of the conformers C_1, C_3 and C_4 are in the range 47.9–48.64 kJ mol^{-1} which are higher than those of C_2 (43.4kJ/mol) and C_5 (41.22 kJ/mol). The relative energy of the C_5 ion pair conformer (3.53 kJ.mol) is lower than that of the ion pair conformers of C_1 (4.03 kJ/mol) and C_2 (5.17 kJ/mol) and thus is expected to be more stable than the other two. However, the question why the C_5 ion pair conformer has less absolute interaction energy than C_1 and C_2 ion pair conformers is likely to be raised. From **Table 2**, it is obvious that the C_1 ion pair conformer, has multiple shorter and more linear H-bond interactions such as front-me $C_1{-}H_1{---}O_1$ (with a distance 2.33 Å and an angle of 134.91°), terminal methyl $C_5{-}H_8{---}O_1$ (with a distance 2.57Å and an angle of 140.09°), terminal methyl $C_6{-}H_9{---}N_1$ (with a distance 2.58 Å and an angle of 142.77°) interactions whereas the C_3 ion pair conformer has longer and nonlinear hydrogen bonds such as front-me $C_1{-}H_1{---}O_1$ (with a distance 2.79Å and an angle of 97.45°), terminal methyl $C_5{-}H_8{---}O_1$ (with a distance of 2.55Å and an angle of 137.24°), terminal methyl $C_6{-}H_9{---}N_1$ (with a distance 2.64Å and an angle of 130.27°) H-bond interactions. In C_5 ion pair conformer, the strongest H-bond is made between front-me $C_1{-}H_1{---}O_1$ (with a distance 2.18Å and an angle of 145.72°), terminal methyl $C_5{-}H_8{---}O_1$ (with a distance 2.42Å and an angle of 150.03°), front-but $C_1{-}H_1{---}O_3$ (with a distance 2.39Å and an angle of 118.63°), methylene $C_2{-}H_2{---}O_3$ (with a distance 2.63Å and an angle of 114.59°), terminal methyl $C_5{-}H_8{----}F_1$ (with a distance 2.89Å and an angle of 155.72°) H-bond interactions (see **Table 2** and **Figure 6**). The results show that the greater the number of multiple H-bond interactions, the greater the absolute value of the interaction energy.

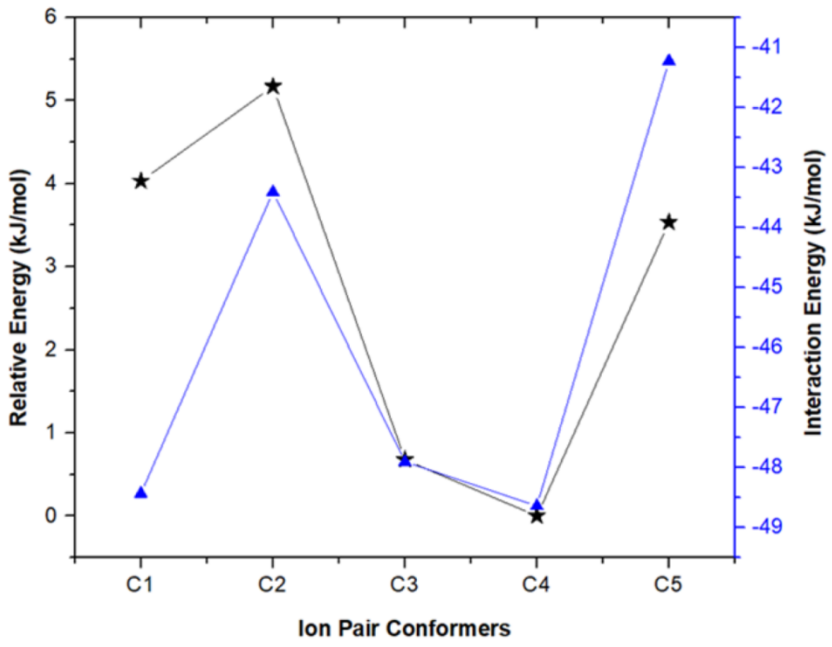

Figure 7: Correlation between interaction and relative conformer energies of the different ion pair conformers of [EMI][TFSI] ion pairs in dielectric continuum medium using ωB97x-D/DGDZVP level of theory and basis set.

3.3 The Stabilization Energies of [EMI][TFSI] Ion Pair Conformers.

Natural bond orbital analysis (NBO) [119] provides good information regarding the change in charge densities of donor and acceptor ions. While the interaction energy is defined as the difference between the energy of the ion pairs and the sum of the energies of the purely cationic and anionic species (**Equation 1**) [120] however**,** for each donor NBO(i) and acceptor NBO(j), the stabilization energy E(2) (**Equation 2**) associated with delocalization of electron pair from donor orbital (i) to acceptor orbital (j) and is estimated as:

$$E(2) = \Delta E_{ij} = \frac{q_i F(i,j)^2}{\varepsilon_i - \varepsilon_j} \qquad (2)$$

Where q_i is the donor orbital occupancy, ε_i and ε_j are the diagonal elements (orbital energies) and F(i,j) is the interaction element between donor and acceptor orbitals and is known as diagonal NBO Fock matrix element. In this case, the electronic wave function is interpreted in terms of a

set of occupied Lewis and a set of unoccupied non-Lewis localized orbital and the delocalization effects can be identified by means of off-diagonal elements of the Fock matrix. The forces of these delocalization interaction, E(2) (kcal/mol), are estimated by second order perturbation theory [121]. When electrons are shared via the $Y_{lp} \rightarrow \sigma^*_{C-H}$ (Y = N, O, or F) bonding and anti-bonding interaction, this is equivalent to transferring electron density from the lone pair of N and/or O atoms into the σ^*_{C-H} orbital. Typically $Y_{n(lp)} \rightarrow \sigma^*_{X-H}$ is strongest for a linear or near linear H-bond. In particular, the H-bond strength has been related to the charge transfer component $E^{(2)}n \rightarrow \sigma^*$ of the NBO analysis. $E^{(2)}n \rightarrow \sigma^*$ is proportional to the amount of electron density (qi) donated from the filled donor lone-pair orbital into the empty σ* orbital, moderated by the energy difference between these two fragment orbitals (Δε), and thus the NBO analysis on the DFT optimized structure allows the analysis of intermolecular donor–acceptor orbitals interactions [121].

NBO analysis of the structure of various alkyl-imidazolium derivatives with simple mono-atomic anions were studied at B3LYP level with DGDZVP basis set [121]. However, there are no prior reported studies on the detailed NBO analysis of [EMI][TFSI] ion pair conformers that have multiple interactions sites for the anion. In this paper, we are reporting for the first time how stabilization energy obtained from NBO analysis of different ion pair conformers of [EMI][TFSI] helps to get the details of orbital interactions between the empty σ^*_{C-H} fragment orbital (FO) of the $[EMI]^+$ cation and the occupied lone pair FO on N and O of the $[TFSI]^-$ anion at ωB97X-D level using the DGDZVP basis set and the presence of dielectric continuum medium, and the results are compiled in **Tables S9-S12**. Imidazolium based ion pairs with weak H-bond acceptor anions such as $[BF_4]^-$ and $[PF_6]^-$ have $E(2)_n \rightarrow_{\sigma^*}$ = 50-60 kJ/mol while those with strong hydrogen acceptor anions such as Cl^- and $[NO_3]^-$ have $E(2)_n \rightarrow_{\sigma^*}$ = 110-180 kJ/mol. The much stronger hydrogen bonds of protic ion pairs with strong hydrogen acceptor anions of $[NO_3]^-$ have $E(2)_n \rightarrow_{\sigma^*}$ = 250-320 kJ/mol [113, 123]. Generally speaking, weak H-bonds have $E(2)_n \rightarrow_{\sigma^*}$ < 30 kJ/mol and strong hydrogen bonds have $E(2)_n \rightarrow_{\sigma^*}$ > 150 kJ/mol [113] and those lying between these extremes are moderate hydrogen bonds. However, it is still the subject of scientific debate an ongoing research to establish a more robust level of knowledge relating to the $E(2)_n \rightarrow_{\sigma^*}$ parameter with respect hydrogen bonds in ionic liquids. In particular, a large range

of IL ion pair conformers need to be examined, geometric influences and the impact of multiple concomitant hydrogen bonds need be better understood.

Table 3: Hydrogen bond length, angle and stabilization energies (**$E(2)_n \rightarrow \sigma^*$ (kcal/mol))** of the different conformers of [EMI][TFSI] ion pairs in dielectric continuum medium using ωB97x-D/ DGDZVP level of theory and basis set.

Conformer	**C_1**	**C_2**	**C_3**	**C_4**	**C_5**
H-bond Length(Å)					
C1-H1---O1	2.33307	2.40054	2.79484	2.51111	2.17586
C5-H8----O1	2.56533	2.55313	2.76501	2.42109	2.42161
C2-H2---O3	2.79919	3.16777	2.41806	2.57019	2.63206
C1-H1---N1	2.8076	2.84439	2.63625	2.61455	3.78727
C6-H9--N1	2.58145	4.98124	2.6368	2.55063	5.06497
C2-H2---N1	3.83064	2.75629	2.9609	3.68491	5.07138
C6-H9----F3	2.83018	4.7277	2.72126	2.73334	2.82859
H-bond Angle(deg)					
C1-H1---O1	134.90792	122.62125	97.45009	130.00118	145.72274
C5-H8----O1	140.08964	137.23789	97.2522	149.85344	150.0253
C2-H2---O3	113.78501	83.05732	145.26464	127.16128	114.59376
C1-H1---N1	95.12519	88.8275	106.60753	98.23770	139.06389
C6-H9--N1	147.94347	75.4204	130.27446	144.1511	135.42838
C2-H2---N1	84.28362	121.46653	106.40545	85.42306	121.53507
C6-H9----F3	142.77348	97.68907	120.32157	138.0436	155.72293
$E(2)_n \rightarrow \sigma^*$ (kcal/mol)					
$O_1 \rightarrow \sigma^*_{C1\text{-}H1}$	1.66	0.64	0.00	0.61	2.15
$O_1 \rightarrow \sigma^*_{C5\text{-}H8}$	0.64	0.44	0.57	0.80	0.88
$O_3 \rightarrow \sigma^*_{C2\text{-}H2}$	0.14	0.00	1.24	0.26	0.33
$N_1 \rightarrow \sigma^*_{C1\text{-}H1}$	0.00	0.00	0.00	0.00	0.00
$N_1 \rightarrow \sigma^*_{C6\text{-}H9}$	1.28	0.00	0.00	0.89	0.00
$N_1 \rightarrow \sigma^*_{C2\text{-}H2}$	0.00	0.38	0.00	0.00	0.00
$F_3 \rightarrow \sigma^*_{C6\text{-}H9}$	0.08	0.00	0.07	0.05	0.13

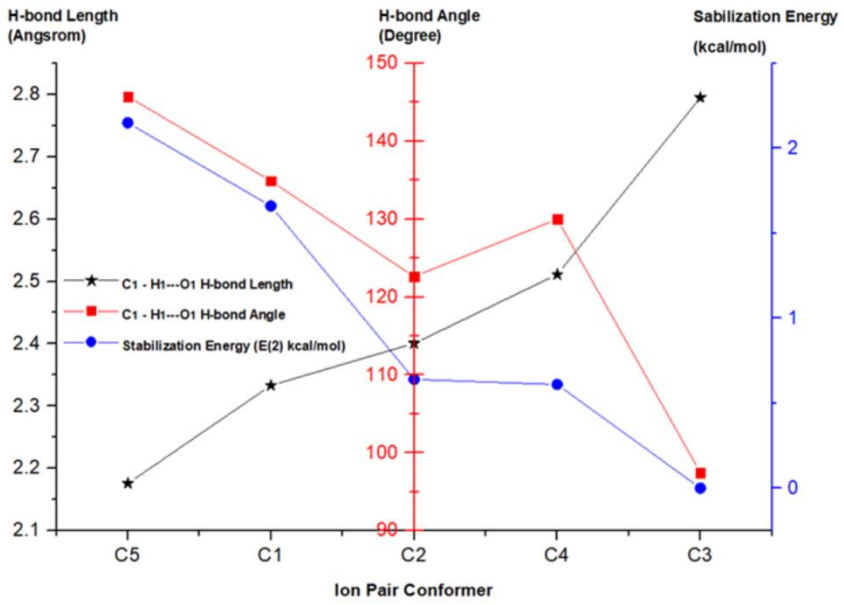

Figure 8: Correlations between H-bond length ($C_1-H_1---O_1$), H-bond angle ($<C_1-H_1---O_1$) and stabilization energies (E(2)) of the different ion pair conformers.

From the **Tables S9-S12**, we observed that in general, for [EMI][TFSI] ion pair conformers, charge transfer occurs mainly from the lone pairs of oxygen and nitrogen atom to the σ-type anti-bonding orbital of the C–H and π-type anti-bonding orbitals of N-C bonds. This was evident from the values of the stabilization energy E(2) associated with each electron delocalization from the donor to acceptor orbitals. Apparently, from the above results, it is noticeable that there exist large numbers of multiple concomitant hydrogen bonds but the values of the stabilization energy E(2) are generally small ($E(2)_{n\rightarrow\sigma^*}$ < 3 kcal/mol) for the individual H-bond interactions. The shorter the C–H---O and/or C–H---N bond is, the larger charge transfer, and the larger the stabilization energy E(2) associated with electron delocalization from donor to acceptor anti-bonding orbital (see **Figure 8**). For example, we can see from **Table 2** and **Table 3** that there is a strong linear correlation between H-bond length and the value of the stabilization energy (E(2)). The ion pair conformer C_5 has the shortest $C_1–H_1---O_1$ bond (2.18 Å) and more linear angle (145.72°), and thus with greater value of second-order perturbation energy for $O_1\rightarrow\sigma^*_{C1\text{-}H1}$ (E(2) = 2.15 kcal/ mol) among all ion pair conformers investigated. The ion pair conformer C_1 (with $C_1–H_1---O_1$ bond length 2.33 Å and angle 134.91°) has the second largest stabilization energy for $O_1\rightarrow\sigma^*_{C1\text{-}H1}$ (E(2) = 2.15 kcal/ mol) followed by C_2 (with $C_1–H_1---O_1$ bond length 2.40 Å and angle 122.62125°) and C_4 (with $C_1–H_1---O_1$ bond length 2.51 Å and angle 130.00°). NBO

analysis of [EMI][TFSI] ion pair conformers also revealed that the lone pairs of nitrogen donate its electrons to the σ-type and π-type anti-bonding orbital for N_1–C_1 bonds. The weak NBO interactions of $N_1 \rightarrow \sigma^*_{N1\text{-}C1}$ and $N_1 \rightarrow \pi^*_{N1\text{-}C1}$ imply the existence of anion donor - π* interactions. Other non-bonded interactions that also contribute significantly to stabilization of the compound are $O_1 \rightarrow \sigma^*_{C5\text{-}H8}$, $O_3 \rightarrow \sigma^*_{C2\text{-}H2}$, and $N_1 \rightarrow \sigma^*_{C6\text{-}H9}$ interactions.

The [EMI][TFSI] ion pair conformers tend to form multiple but bent H bonds, reducing the strength of the individual H bonds from a potential (linear) maximum. Generally speaking, they form a major H-bond with the C_1–H_1 and a minor one with C_{alkyl}–H bonds. The relative contribution from each of these is not easily resolved via the association energy which includes the ionic as well as a combined H-bond contribution. Moreover, [EMI][TFSI] ion pairs are not symmetric and thus cannot reach the maximum covalent contribution, which is possible only for symmetric H-bonds. From **Table 3**, it is clear that the most significant E(2) values for C_1 ion pair conformer are for the LP(2)O_1 (donor NBO)→BD*(1)C_1–H_1 (acceptor NBO) interaction with an E(2) of 1.66 kcal/mol that shows the presence of weak C_1–H_1---O_1 H-bond interaction; LP(1)N_1(donor NBO) →BD*(1)C6–H9 (acceptor NBO) interaction with an E(2) of 1.28 kcal/mol that shows the presence of weak C_1–H_1---N_1 H-bond interaction; and LP(2)N_1 (donor NBO) →BD*(2)N1-C1 (acceptor NBO) interactions with an E(2) of 1.78 kcal/mol indicating the presence of anion donor - π* acceptor interactions while the rest are less significant in comparison to this value. For the C_1 ion pair conformer (**Table S12**), the stabilization energies that arise from LP(2)O_1(donor NBO) →BD*(1)C_1–H_1(acceptor NBO) is only with an E(2) value of 0.61 kcal/mol and LP(1) N_1(donor NBO) →BD*(1) N_1– C_1 (acceptor NBO) interaction with an E(2) of 2.32 kcal/mol indicating the presence of anion donor - π* acceptor interactions. For the C_4 ion pair conformer, however, the E(2) values have much smaller values for C_1–H_1 and C_6–H_9 interaction indicating the absence of appreciable C–H---O_1 H-bond interaction. In the C_4 ion pair conformer, the E(2) value for anion donor - π* acceptor interactions is much larger than other interactions. The C_2 ion pair conformer (**Table S13**) which has the cation ethyl group in anti-position with respect to the position of the anion in the imidazolium ring (see **Figure 4**), has LP(2)O_1(donor NBO) →BD*(1)C_1–H_1(acceptor NBO) interaction with an E(2) of 0.64 kcal/mol indicating the absence of appreciable C_1 – H_1---O_1 H-bonding interaction; LP(2)N_1 (donor NBO) →BD*(2)N_1–C_1 (acceptor NBO) interactions with an E(2) of 1.38 kcal/mol indicating the

presence of anion donor - π* acceptor interaction. The C_3 ion pair conformer (**Table S14**) which has the cation ethyl group in syn-position with respect to the position of the anion in the imidazolium ring, has LP(2)O_3 (donor NBO) →BD*(1) C_2−H_2 (acceptor NBO) interactions with an E(2) of 1.24 kcal/mol indicating the presence of C_2−H_2 ---O_3 H-bonding interaction through the ethyl group hydrogen of the cation. The C_5 ion pair conformer (**Table S15**) has LP(1) O_1(donor NBO) →BD*(1)C_1−H_1(acceptor NBO) interactions with an E(2) of 2.15 kcal/mol and LP(2)O_1(donor NBO) →BD*(1)C_1−H_1(acceptor NBO) interactions with an E(2) of 1.34 kcal/mol indicating the presence of C_1−H_1---O_1 H-bonding interaction.

The NBO method has also been employed to characterize the natural orbital coefficients and hybridization on H-bond formation. The main listing of NBOs, displaying occupancy, natural atomic hybrids, polarization coefficient, and sp^{λ} composition of the different conformers of [EMI][TFSI] ion pair for a selected set of NBOs are shown in **Table 4** and **Figure 9**. For the ion pair conformer C_1, the $\sigma^*_{C1\text{-}H1}$ NBO is formed from an $sp^{1.63}$ hybrid (61.95% p-character) on carbon interacting with an s orbital (100% s-character) on hydrogen corresponding to linear combination of atomic orbitals $0.609C(sp^{1.63}) - 0.794H(s)$ comprising 61.95% p-character and larger polarization coefficient of H. This result can be substantiated by the extent of orbital interaction between lone pair orbitals LP(1) and LP(2) of O_1 and the anti-bonding orbitals of $\sigma^*_{C1\text{-}H1}$. The lone pair electron of LP(2) ($sp^{1.00}$ hybride orbital with 99.72% p-character) is actually oriented along the direction of the O_1−H_1 H-bond axis. The LP(1) of O_1 (which has $sp^{0.34}$ hybrid orbital with 74.79% s character and 25.19% p characer) possesses a vintage overlap with the $\sigma^*_{C1\text{-}H1}$ orbital, while the interaction of the LP(2) orbital of O_1 with the $\sigma^*_{C1\text{-}H1}$ anti-bonding orbital is relatively larger. Furthermore, the percentage of ”s” character of the lone pair orbital is another factor that determines the strength of H-bond interaction. The NBO analysis indicates that the ”s” character of LP(1) of O_1 (74.79%) is greater than that of LP(2) orbital. While, the “p” character of LP(2) are higher than that of LP(1) on O_1. Hence, the LP(1) should be more tightly held by the nucleus and reduced tendency for hyper conjugative charge transfer. Similarly, the $\pi^*_{N1\text{-}C1}$ NBO is formed from an $sp^{99.99}d^{26.92}$ hybrid (99.69% p-character) on carbon interacting with an $sp^{1.00}$ hybrid orbital (99.93% p-character) on nitrogen corresponding to the linear combination of the orbitals $0.8461C(sp^{99.99}d^{26.92}) - 0.5330N(sp^{1.00})$ comprising $sp^{1.00}$ hybrids (99.93% p-character) and larger polarization coefficient of C. The NBO analysis indicates that the ”s” character of LP(1) (43.15%) is greater than that of the ”s” character LP(2) of N_1 (0.00%)

(see **Table 4** and **Figure 9**. The "p" characters of LP(2) are higher than that of LP(1) on N1 indicating that the LP(1) should be more tightly held by the nucleus and reduced tendency of hyper conjugative charge transfer. The natural bond orbital (NBO) interactions of the different conformers $C_2 - C_5$ of [EMI][TFSI] ion pairs are shown in **Figure 9**.

Table 4: Selected natural bond orbital (NBO), occupancy, natural atomic hybrids, polarization coefficient, and sp^{λ} composition of the different conformers of [EMI][TFSI] ion pairs.

Conformer	**NBO**	**Occupancy**	**Energy (a.u.)**	**Coefficients**	**Hybrids**	**AO%**
C1	LP(1) O1	1.98052	-0.90439		$sp^{0.34}$	s(74.79%)p(25.19%)d (0.02%)
	LP(2) O1	1.82785	-0.39580		$sp^{1.00}$	s(0.00%)p (99.72%)d (0.28%)
	LP(1) N1	1.88524	-0.52876		$sp^{1.30}$	s(43.45%)p(56.32%)d (0.23%)
	LP(2) N1	1.77160	-0.35457		$sp^{1.00}$	s(0.00%)p (99.74%)d (0.25%)
	BD*(1)C1 - H1	0.01663	0.58538	0.6086C (37.03%)	$sp^{1.63}$	s(38.01%)p (61.95%)d (0.04%)
				-0.7935H (62.97%)	s	s(100.00%)
	BD*(1) C6-H9	0.00969	0.59638	0.6236C (38.89%)	$sp^{3.08}$	s(24.50%)p (75.43%)d (0.07%)
				-0.7817H (61.11%)	s	s(100.00%)
	BD*(1) N1-C1	0.02789	0.56533	0.7952C (63.23%)	$sp^{2.20}$	s(31.22%)p(68.61%)d (0.17%)
				-0.6064 N (36.77%)	$sp^{1.97}$	s(33.67%)p(66.29%)d (0.05%)
	BD*(2) N1-C1	0.50690	-0.01431	0.8461C (71.60%)	$sp^{99.9}d^{26.9}$	s(0.01%)p(99.69%)d(0.30%)
				-0.5330N (28.40%)	$sp^{1.00}$	s(0.00%)p (99.93%)d (0.06%)
C2	LP(1) N1	1.88448	-0.52792		$sp^{1.31}$	s(43.15%)p (56.62%)d (0.23%)
	LP(2) N1	1.77143	-0.35310		$sp^{1.00}$	s(0.00%)p(99.75%)d (0.25%)
	BD*(1) N1-C1	0.02643	0.57057	0.7956C (63.30%)	$sp^{2.17}$	s(31.51%)p(68.32%)d (0.17%)
				-0.6058N (36.70%)	$sp^{1.96}$	s(33.73%)p(66.22%)d (0.05%)
C3	LP(1) O3	1.98266	-0.89949		$sp^{0.34}$	s(74.69%)p(25.29%)d (0.02%)
	LP(2) O3	1.82297	-0.39034		$sp^{1.00}$	s(0.00%)p(99.72%)d (0.28%)
	BD*(1) C2-H2	0.01421	0.60541	0.6176C (38.15%)	$sp^{3.03}$	s(24.81%)p(75.11%)d (0.09%)
				-0.7865H (61.85%)	s	s(100.00%)
C4	LP(1) N1	1.89527	-0.53058		$sp^{1.01}$	s(49.54%)p(50.27%)d (0.19%)
	LP(2) N1	1.77213	-0.35456		$sp^{99.9}d^{11.35}$	s(0.02%)p(99.74%)d(0.24%)
	BD*(1) N1-C1	0.02796	0.56805	0.7956C (63.30%)	$sp^{2.20}$	s(31.25%)p(68.59%)d (0.17%)
				-0.6058N (36.70%)	$sp^{1.98}$	s(33.54%)p(66.41%)d (0.05%)
C5	LP(1) O1	1.98400	-0.90507		$sp^{0.34}$	s(74.57%)p(25.41%)d (0.02%)
	LP(2) O1	1.81937	-0.40112		$sp^{1.00}$	s(0.00%)p(99.70%)d (0.30%)
	BD*(1)C1 - H1	0.01867	0.59123	0.6075C (36.91%)	$sp^{1.62}$	s(38.22%)p(61.74%)d (0.04%)

	-0.7943H (63.09%)	s	s(100.00%)

"LP" for 1-center valence lone pair, "BD" for 2- center bond, "BD*" for 2-center antibond, and, the unstarred and starred labels corresponding to Lewis and non-Lewis NBOs, respectively), a serial number (1, 2,... if there is a single, double,... bond between the pair of atoms), and the atom(s) to which the NBO is affixed.

NBO analyses for [EMI][TFSI] ion pair conformers were performed to obtain the NBO charge distribution (**Table. S9 - S12**). For the C_1 ion pair conformer, the NBO charge of H_1 (0.25476) is more positive than that of other hydrogen atoms, while the NBO charges of O_1 (-0.98636) is more negative than that of other oxygen/fluorine atoms, which is ascribed stronger to C_1–H_1---O_1 H-bond interactions (E(2)=1.66 kcal/mol**)**. Similarly, for the C_3 ion pair conformer, the most negative charge of O_3 (-0.97992) and the C_2-H_2---O_3 interaction leads to the more positive charge of H_2 (0.23535). The C_5 ion pair conformer has the most positive H atom (0.25638) which is ascribed to the shorter distance of C_1-H_1---O_1 H-bond interactions (E(2)= 2.15 kcal/mol). Analysis of NBO charges (see **Table S9 – S12**) show that the positive charge of H and negative charge of O atoms increase when they are involved in C-H···O interactions. Generally speaking, the shorter the H-bond length of C-H···O, the larger the increase of positive charges of hydrogen atoms and negative charges of oxygen. The anion donor π-type anti-bonding interaction between the most electronegative N_1 atom of the $[TFSI]^-$ anion with the π^*_{N1-C1} anti-bonding orbital of the $[EMI]^+$ cation leads to more positive charges on C_1 atoms of the C_1(0.3303), C_2 (0.34646) and C_4 (0.34389) ion pair conformers. The greater the magnitude of the anion donor π^*_{N1-C1} anti-bonding interaction, the higher the values of the positive charges on C_1 atoms of the $[EMI]^+$ cation.

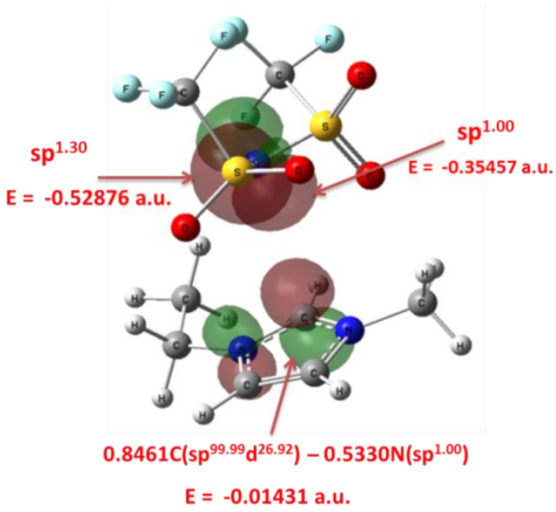
sp1.30
E = -0.52876 a.u.
sp1.00
E = -0.35457 a.u.
0.8461C(sp99.99d26.92) – 0.5330N(sp1.00)
E = -0.01431 a.u.

(a)

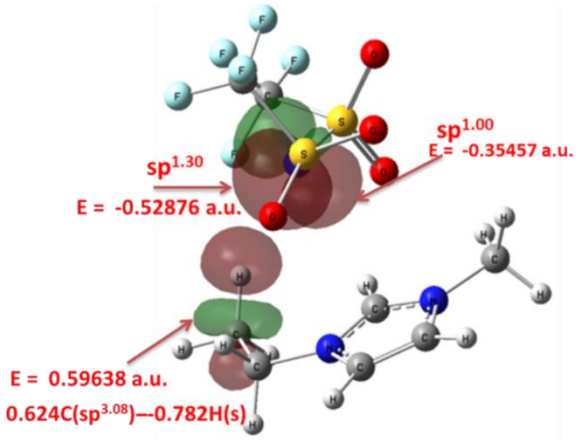
sp1.00
E = -0.35457 a.u.
sp1.30
E = -0.52876 a.u.
E = 0.59638 a.u.
0.624C(sp3.08)–-0.782H(s)

(b)

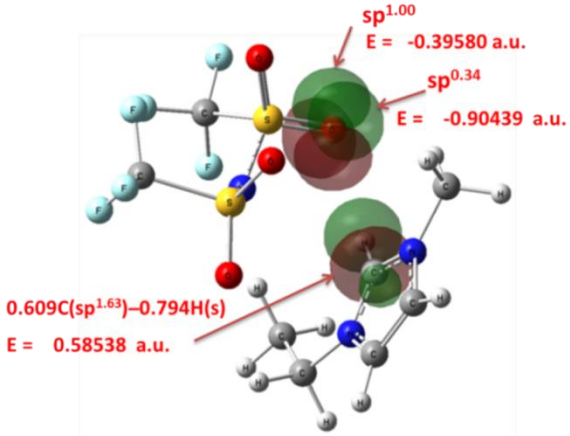
sp1.00
E = -0.39580 a.u.
sp0.34
E = -0.90439 a.u.
0.609C(sp1.63)–0.794H(s)
E = 0.58538 a.u.

(c)

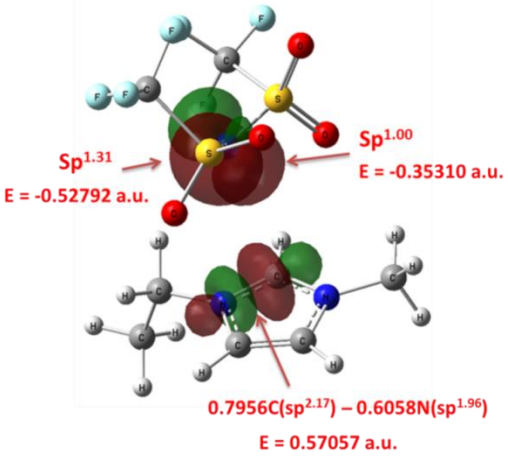
Sp1.31
E = -0.52792 a.u.
Sp1.00
E = -0.35310 a.u.
0.7956C(sp2.17) – 0.6058N(sp1.96)
E = 0.57057 a.u.

(d)

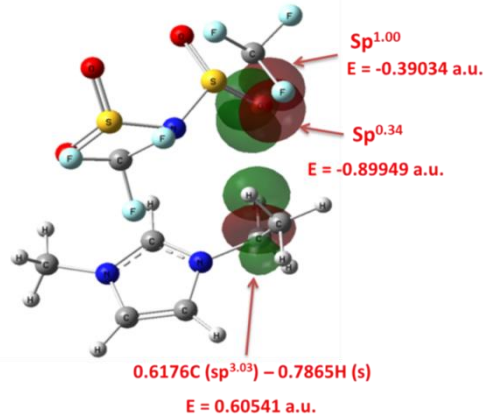
Sp1.00
E = -0.39034 a.u.
Sp0.34
E = -0.89949 a.u.
0.6176C (sp3.03) – 0.7865H (s)
E = 0.60541 a.u.

(e)

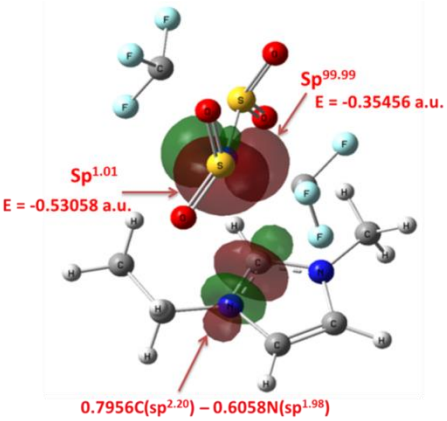
Sp99.99
E = -0.35456 a.u.
Sp1.01
E = -0.53058 a.u.
0.7956C(sp2.20) – 0.6058N(sp1.98)

(f)

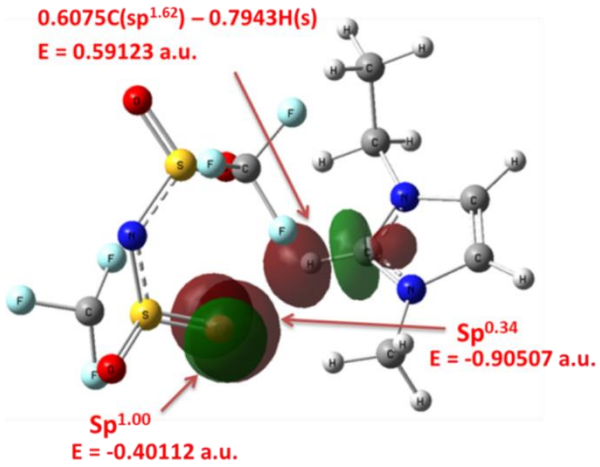

(g)

Figure 9: Selected natural bond orbital (NBO) interactions between (a) LP(1)N1, LP(2)N1 and BD*(2)N1-C1 for C1 (b) LP(1)N1, LP(2)N1 and BD*(1) C6-H9 for C1 (C) LP(1)O1, LP(2)O1 and BD*(1)C1-H1 for C1 (d) LP(1)N1, LP(2)N1 and BD*(1)N1-C1 for C2 (e) LP(1)O3, LP(2)O3 and BD*(1)C2-H2 for C3 (f) LP(1)N1, LP(2)N1 and BD*(1)N1-C1 for C4 (g) LP(1) O1, LP(2)O1 and BD*(1)C1-H1 for C5 of the different conformers of [EMI][TFSI] ion pairs in dielectric continuum medium using ωB97x-D/ DGDZVP level of theory and basis set. "LP" for 1-center valence lone pair, "BD" for 2- center bond, "BD*" for 2-center antibond, and, the unstarred and starred labels corresponding to Lewis and non-Lewis NBOs, respectively), a serial number (1, 2,... if there is a single, double,... bond between the pair of atoms), and the atom(s) to which the NBO is affixed.

3.4 Radial Distribution Functions

Radial distribution functions (RDFs) between the centers of mass of the ions, the solvent and between various atoms of the ions have been calculated in order to study the microstructure of the ILs. Thus, we focus here on the cation–cation, anion–anion, cation–anion, solvent-solvent distribution and the specific atoms comprising the two moieties in order to analyze and provide an insightful average picture of the IL/carbonate structure. **Figure 10** shows the radial pair distribution functions between the (a) geometric ring centers of $[EMI]^+$ (b) geometric ring centers of $[TFSI]^-$ (c) geometric ring centers of [EMI] and[TFSI] (d) geometric ring centers of [EC] and (f) geometric ring centers of [DMC] at 298 K and 1 atm.

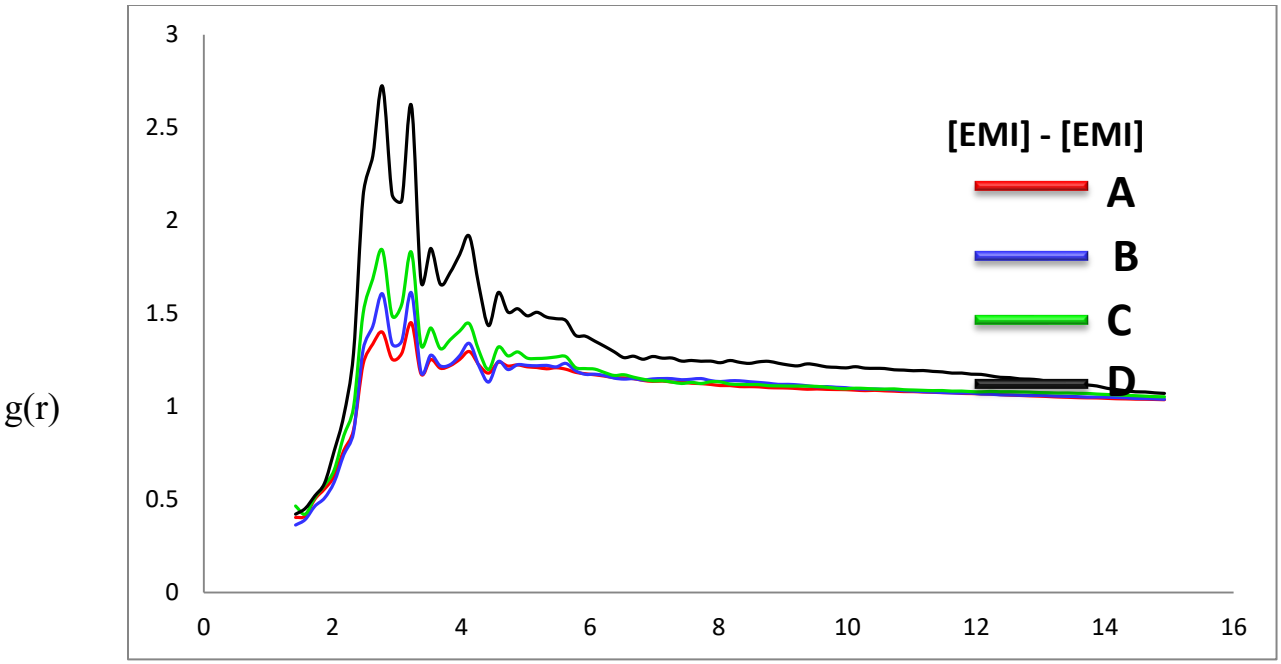
g(r)
3
2.5
2
1.5
1
0.5
0
0
2
4
6
8
10
12
14
16
[EMI] - [EMI]
A
B
C
D
r(Å)

(a)

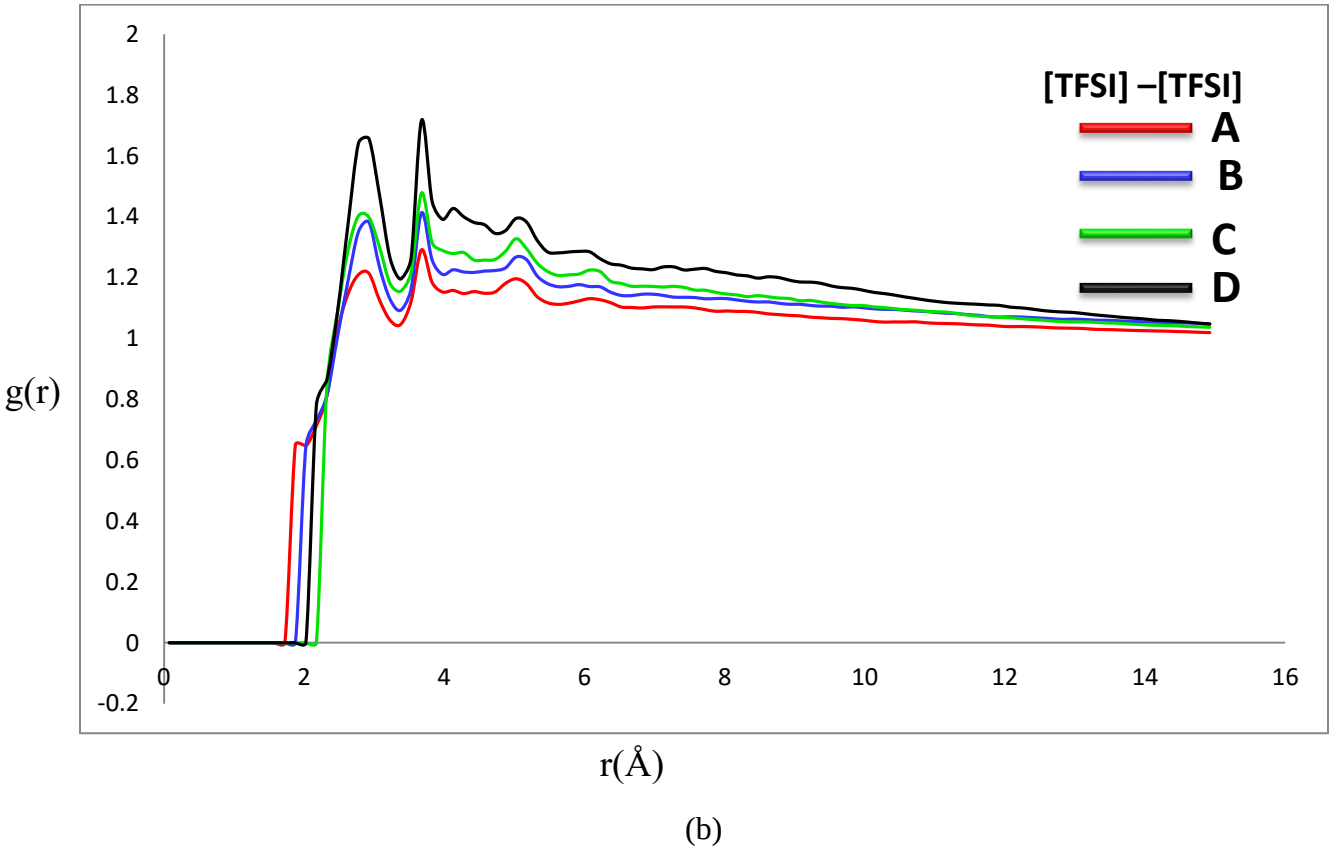
g(r)
2
1.8
1.6
1.4
1.2
1
0.8
0.6
0.4
0.2
0
-0.2
0
2
4
6
8
10
12
14
16
[TFSI] –[TFSI]
A
B
C
D
r(Å)

(b)

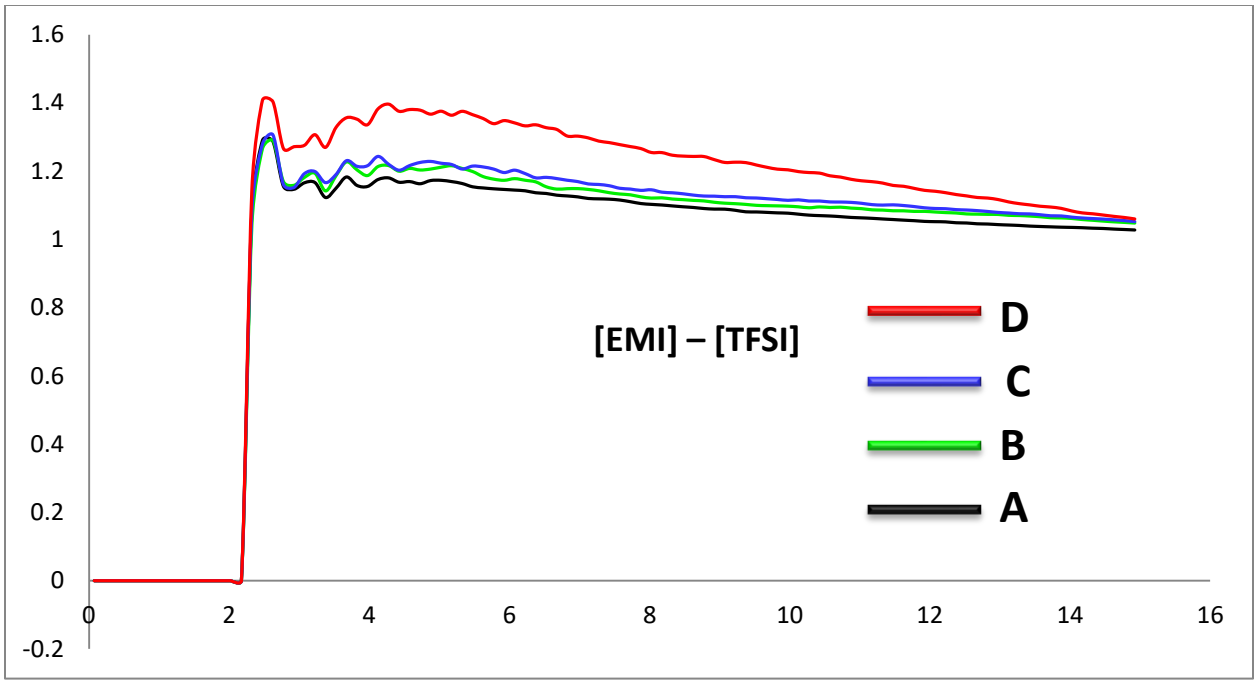
1.6
1.4
1.2
1
0.8
0.6
0.4
0.2
0
-0.2
0
2
4
6
8
10
12
14
16
[EMI] – [TFSI]
D
C
B
A

g(r)

(C) r(Å)

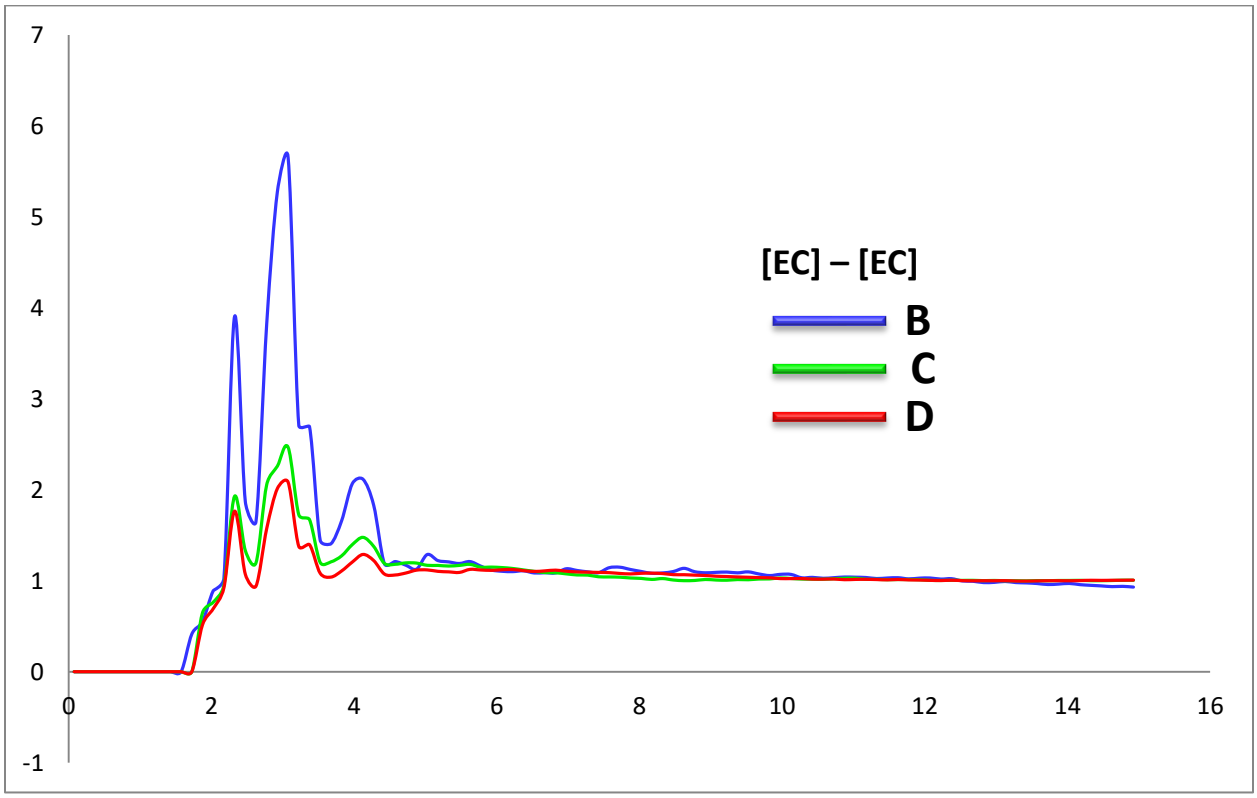
7
6
5
4
3
2
1
0
-1
0
2
4
6
8
10
12
14
16
[EC] – [EC]
B
C
D

g(r)

r(Å)

(d)

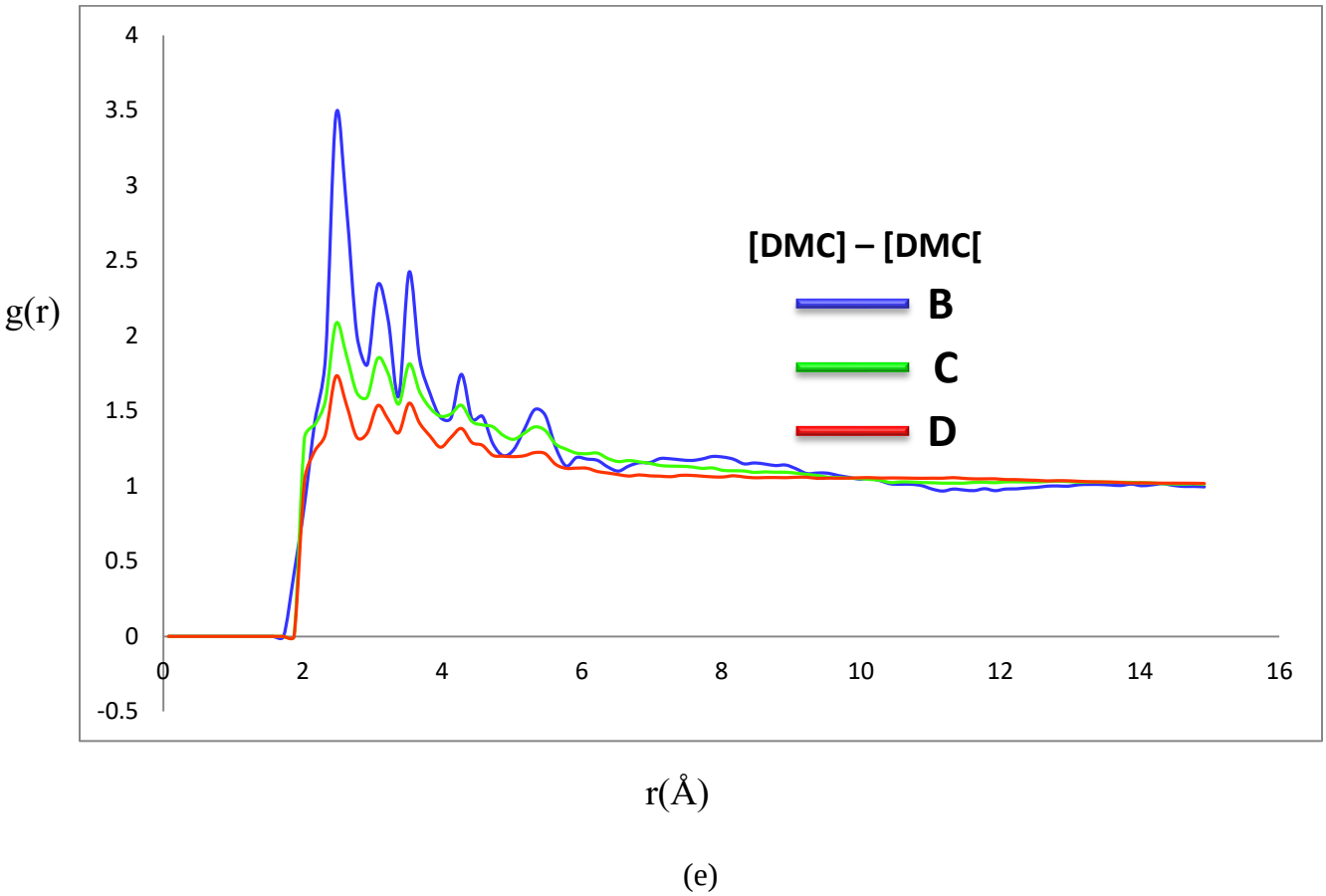

(e)

Figure 10 Radial pair distribution functions between the (a) geometric ring centers of $[EMI]^+$ (b) geometric ring centers of $[TFSI]^-$ (c) geometric ring centers of [EMI] and[TFSI] (d) geometric ring centers of [EC] and (f) geometric ring centers of [DMC] at 298 K and 1 atm.

For the $[EMI]^+$ cation ring centers, very weak but clear ordering can be observed. There seems to be a first shell of neighboring cations at around 250 pm for the pure IL (system A). This finding is different from other previously reported results about simulation studies of more polar and hydrophilic IL 1-ethyl-3-methylimidazolium acetate with water where no clear ordering was observed [124]. Comparing the different systems A, B, C and D that have different levels of ionic liquid/carbonate concentration , the intensity (height) of the peak is increased from system A, B, C to D upon increasing the content of carbonate in the mixture indicating that the ordering between the cations is enhanced by the addition of carbonate in the mixture (**Figure 10(a)**). Our results in this study show that the first maxima of the ring - ring distance appear at smaller distances than for other aromatic systems, e.g. benzene, where the first maximum is found at

around 575 pm [125]. The $[TFSI]^-$ anions show even a weaker ordering towards each other (**see Figure 10(b)**). There appears first and second shell peaks around 250pm and 350pm respectively. Similar to the phenomenon observed for $[EMI]^+$ ring centers, The intensity (height) of the peak for the $[TFSI]^-$ anions center of mass increases from system A, B, C to D indicting the ordering between the center of mass anions is enhanced by the addition of carbonate in the mixture. According to the RDFs and as previously discussed, the addition of EC/DMC solvents into [EMI][TFSI] IL creates a more structured system than the pure [EMI][TFSI] IL system in terms of first peak heights and longer - range higher neighbor shell. The RDF between $[EMI]^+$ and $[TFSI]^-$, which is given in **Figure 10(c),** shows weak but visible structure for system A which is indicated by the distinct black curve at around 247 pm. The height of the peak is enhanced from system A, B, C to D upon increasing the concentration of EC/DMC solvents as indicated by the black, green, blue and red curves. Panels (d) and (e) of **Figure 10** show the radial distribution function for solvent - solvent interaction between center of masses of [EC] - [EC] and [DMC] – [DMC] interactions as a function of IL/carbonate concentration. The RDF for the [EC] - [EC] interaction shows a very clear structure for system B, C and D, which is indicated by the shorter first peak (230 pm) and longer second peak (300 pm) of the blue, green and red curves. However, the RDF for [DMC] – [DMC] interaction shows first larger peak at 247 pm and second shorter peak at 300 pm. The intensity of the peak for [EC] - [EC] interaction is greater than [DMC] – [DMC] because of the higher dielectric constant of EC (hence EC is more polar than DMC) and has less affinity for weakly polar [EMI][TFSI] IL system. The peak heights for both [EC] - [EC] and [DMC] – [DMC] interaction show a marked increase with increase in concentration of carbonates in the mixture. While the solvent–solvent interaction peak is similarly pronounced for EC and DMC, the [EC] - [EC] function only shows a small structure in the first peak, but again exhibits a stronger second neighbor peak. The [DMC] – [DMC] interaction, on the other hand, shows larger first peak but smaller second peak which is due to the presence of methyl side chain groups in DMC which are able to form micro heterogeneous structures, which is nevertheless absent in EC molecules.

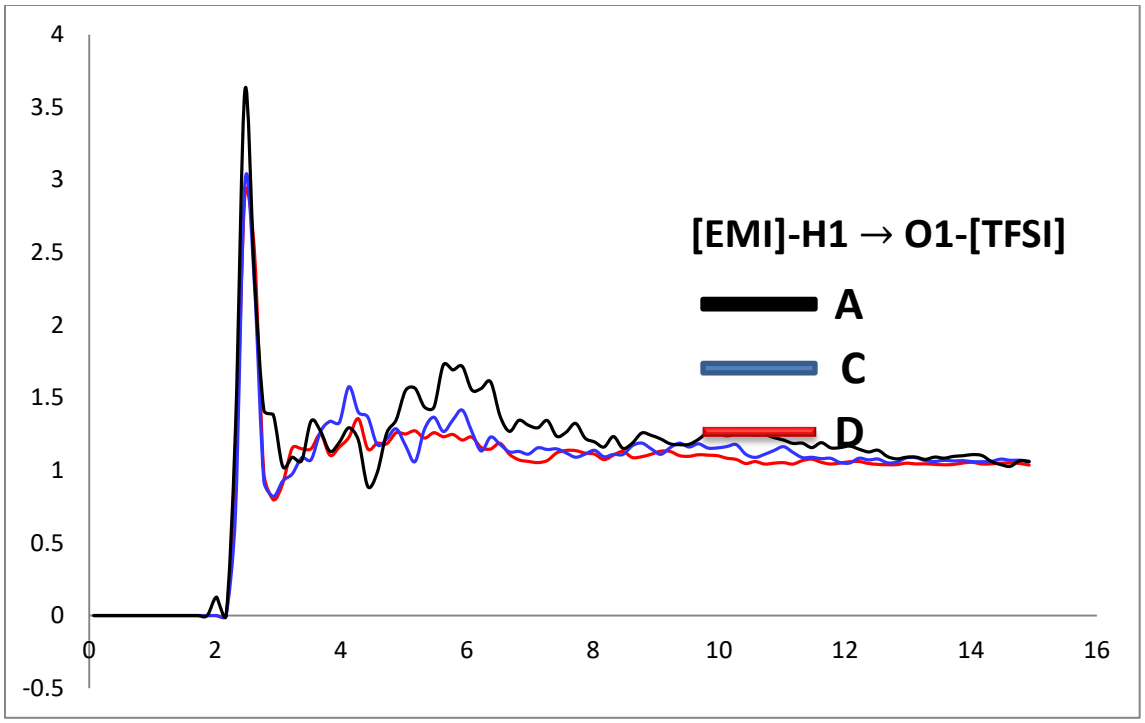
[EMI]-H1 → O1-[TFSI]
A
C
D
4
3.5
3
2.5
2
1.5
1
0.5
0
-0.5
0
2
4
6
8
10
12
14
16

g(r)

r(Å)

(a)

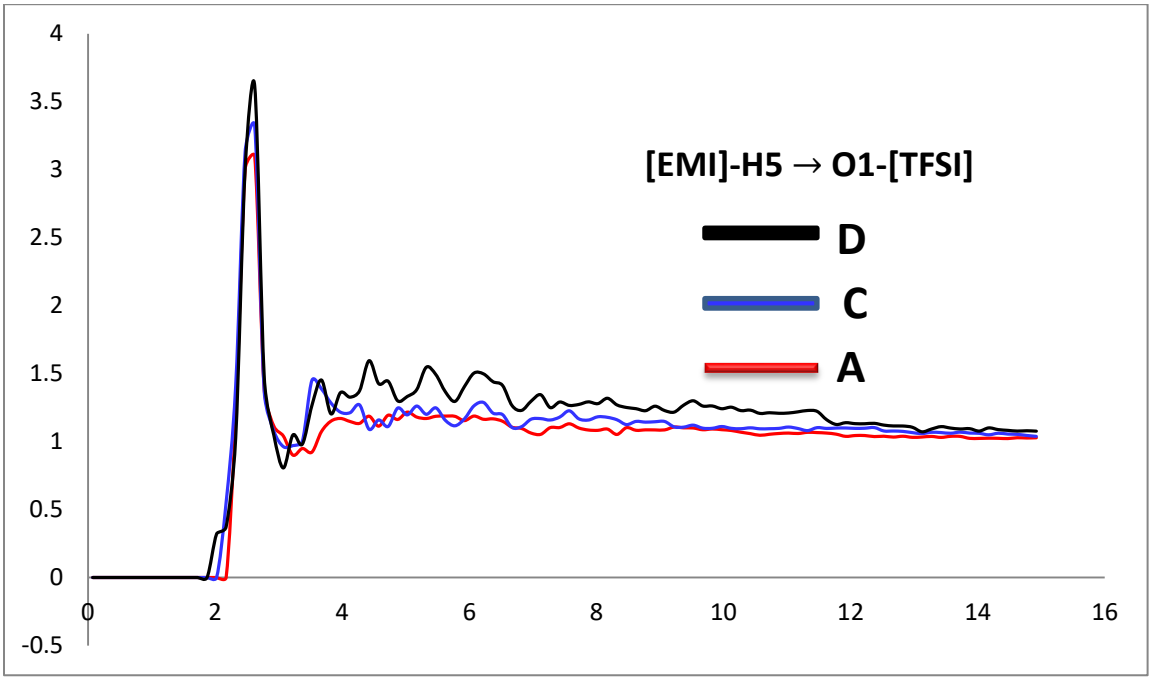
[EMI]-H5 → O1-[TFSI]
D
C
A
4
3.5
3
2.5
2
1.5
1
0.5
0
-0.5
0
2
4
6
8
10
12
14
16

g(r)

r(Å)

(b)

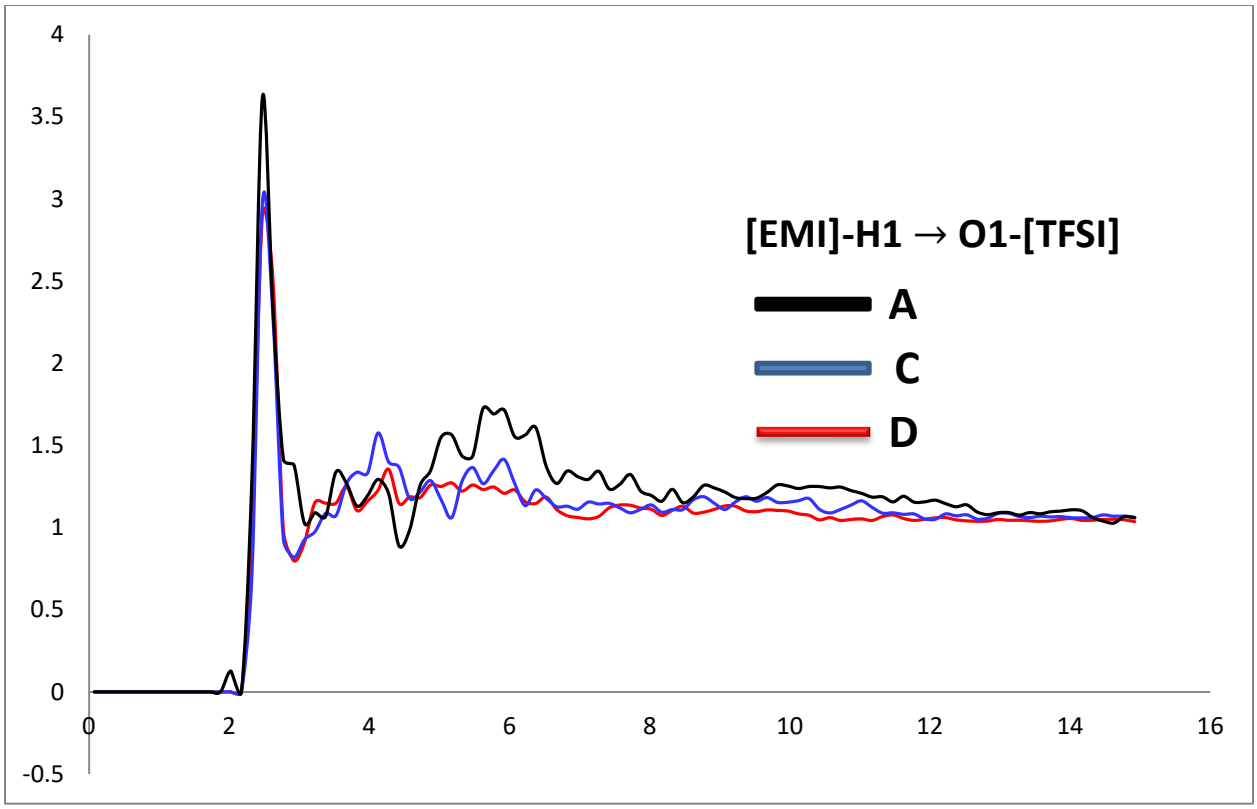
[EMI]-H1 → O1-[TFSI]
A
C
D
g(r)
r(Å)
4
3.5
3
2.5
2
1.5
1
0.5
0
-0.5
0
2
4
6
8
10
12
14
16

(c)

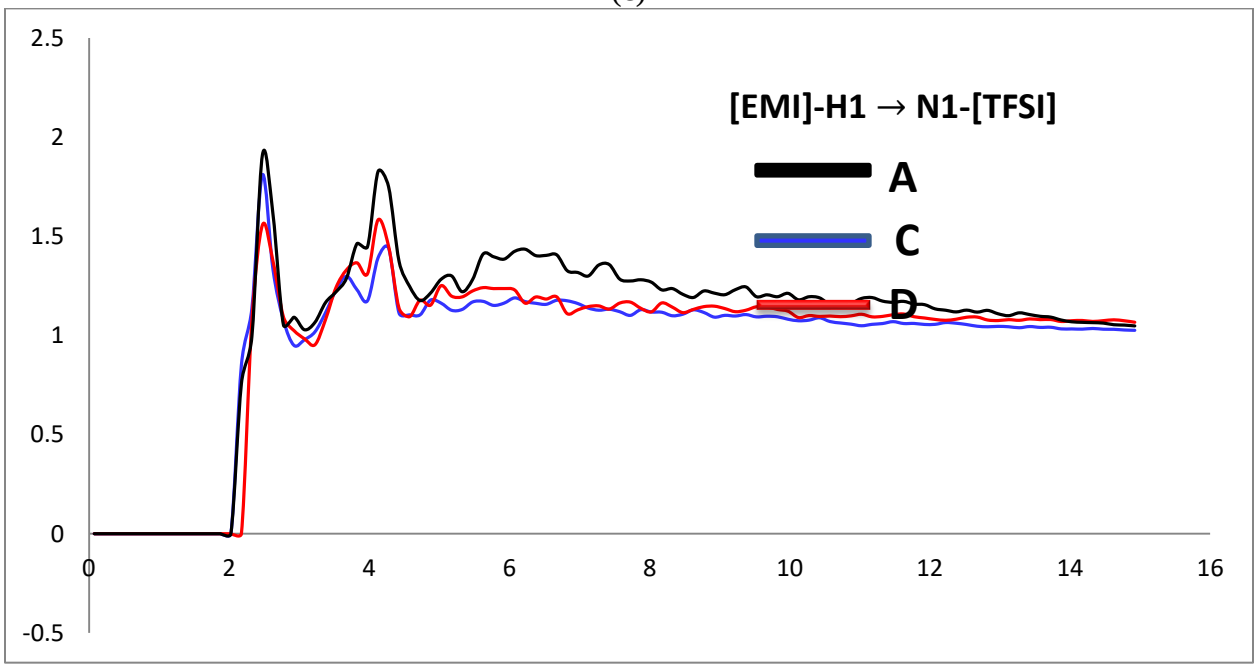
[EMI]-H1 → N1-[TFSI]
A
C
D
g(r)
r(Å)
2.5
2
1.5
1
0.5
0
-0.5
0
2
4
6
8
10
12
14
16

(d)

Figure 11 Radial pair distribution functions between (a) the oxygen (O1) atoms of the $[TFSI]^-$ anion, and the H_1 atom of $[EMI]^+$ cation (b) oxygen (O1) atoms of the $[TFSI]^-$ anion, and the H_5 atoms of $[EMI]^+$ cation (c) nitrogen (N1) atoms of the $[TFSI]^-$ anion, and the H_1 atoms of $[EMI]^+$ cation (d) nitrogen (N1) atoms of the $[TFSI]^-$ anion, and the H_5 atoms of $[EMI]^+$ cation.

The RDFs between nitrogen (N_1) and oxygen (O_1) atoms of the $[TFSI]^-$ anion, and the H_1 and H_5 atoms of $[EMI]^+$ cation are given in **Figure 11**. Panel (a) of **Figure 11** presents the RDFs between the H_1 atom of the $EMI]^+$ cation ring and the oxygen atom O_1 of the $[TFSI]^-$ anion for different fractions of IL/carbonate mixture. It shows a very clear structure for systems A, C and D, which is indicated by the distinct first maximum of the black, blue and red curves at around 247 pm. The first peak is much higher for the pure IL than for system C and D, and the intensity of the peak decreases from A, C to D indicting the interaction between the O_1 atom of $[TFSI]^-$ and H_1 atom of $[EMI]^+$ decreases with increase in carbonate concentration. Panel (b) of **Figure 11** presents the RDFs between the H4/5 atom of the $EMI]^+$ cation ring and the oxygen atom O_1 of the $[TFSI]^-$ anion for different fractions of IL/carbonate mixture. The coordination of the O_1 atom of $[TFSI]^-$ anion to H_4 and H_5 shows distinct maximum as indicated by black, blue and red curves at 260 pm, suggesting the coordination of the anion to the atom H4/5 atom of the $EMI]^+$ cation ring. These findings are in agreement with previous AIMD studies [126] on imidazolium based ionic liquids, where a pronounced coordination of the anion towards the most acidic hydrogen atom of the imidazolium ring was observed as well. By comparing panel (a) with panel (b) of **Figure 11**, it can be seen that the coordination of the O_1 atom of $[TFSI]^-$ anion to the atom H_1 is much more distinct and tighter than for the other two atoms, suggesting that H_1 is a stronger hydrogen bond donor than H_4 and H_5 for the pure IL system (system A). For panel (a), the first peak is much higher for coordination of the O_1 atom of $[TFSI]^-$ anion to the atom H_1 of the$[EMI]^+$ cation for the pure IL than for system D and the height of the first peak is decreased when carbonate is added. In sharp contrast to panel (a), however for panel (b),the first peak is much higher for coordination of the O_1 atom of $[TFSI]^-$ anion to the atom H4/5 of the $[EMI]^+$ cation for system D than for the pure IL (system A) and the height of the first coordination shell increases when carbonate is added. The RDF between H_1 atom of $[EMI]^+$ and N_1 atom of $[TFSI]^-$, which is given in panel (c) of **Figure 11**, shows similar trend. It shows a very clear structure for system A, C and D, which is indicated by the distinct first maximum of the black,

blue and red curves at around 247 and 400 pm. The first peak is much higher for the pure IL (system A) than for system C and D, and the intensity of the peak decreases from A, C to D indicting the interaction between the N_1 atom of $[TFSI]^-$ and H_1 atom of $[EMI]^+$ decreases with increase in carbonate concentration. Panel (d) of **Figure 11** presents the RDFs between the H4/5 atom of the $EMI]^+$ cation ring and the nitrogen atom N_1 of the $[TFSI]^-$ anion for different fractions of IL/carbonate mixture. The coordination of the N_1 atom of $[TFSI]^-$ anion to H_4 and H_5 shows distinct maximum as indicated by black, blue and red curves at 247 pm, suggesting the coordination of the anion to the atom H4/5 atom of the $EMI]^+$ cation ring. By compare panel (c) with panel (d) of **Figure 11**, it can be seen that the coordination of the N_1 atom of $[TFSI]^-$ anion to the atom H_1 is much more distinct and tighter than for the other two atoms, suggesting that H_1 is a stronger hydrogen bond donor than H_4 and H_5 for the pure IL system (system A). For panel (c), the first peak is much higher for coordination of the N_1 atom of $[TFSI]^-$ anion to the atom H_1 of the $[EMI]^+$ cation for the pure IL than for system D and the height of the first coordination shell is decreased when carbonate is added. In sharp contrast to panel (c), for panel (d), the first peak is much higher for coordination of the N_1 atom of $[TFSI]^-$ anion to the atom H4/5 of the $[EMI]^+$ cation for system D than for the pure IL (system A) and the height of the first coordination shell increases when carbonate is added.

3.5 Spatial Distribution Functions

Spatial distribution functions provide an extension of radial distribution functions to the three dimensions of space. **Figure 12** shows spatial distribution functions with the $[EMI]^+$ cation as reference molecule around N_1-C_1-N_2 (see **Figure 1** for atom numbers). For an assignment of colors to atom types and iso-values, please refer to the **Figure 12** subscript. In the pure ionic liquid (system A), adjacent cations are almost exclusively located on top and below the $[EMI]^+$ ring, whereas the $[TFSI]^-$ anions mainly coordinate to the cation within the ring plane. The $[TFSI]^-$ anions occupy both the on top position and in plane position in the $[EMI]^+$ ring. This is in agreement with our DFT based study (**section 3.1 – 3.4**) and RDF based study (**section 3.5**) of [EMI][TFSI] ion pairs, and this finding is in agreement with other recent simulation studies [126-131]. For system B, the obtained results are rather similar to those of system A. With increasing carbonate content (system C and system D), however, it seems that the large amount

of carbonate disturbs the original near ordering which is found in the pure ionic liquid. The H_1 atom of the N_1-C_1-N_2 plane is less populated with $[TFSI]^-$ anions because of the possible competition of EC/DMC with increasing carbonate concentration. This result is substantiated by the RDF based results as shown in in **Figure 11 (a-d)**.

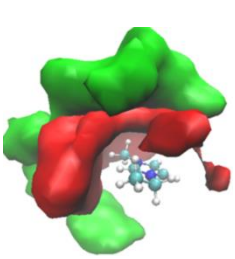

System A: $[EMI]^+$ ISO 1.670 : $[TFSI]^-$ ISO 2.160

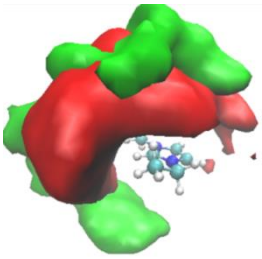

System B: **[**$[EMI]^+$ ISO 1.68 : $[TFSI]^-$ ISO 1.90

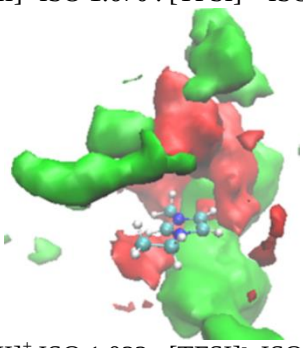

System C: $[EMI]^+$ ISO 1.022 : $[TFSI]^-$ ISO 1.136

System D: $[EMI]^+$ ISO 0.720 : $[TFSI]^-$ ISO 1.421

Figure 12: Spatial distribution functions (SDFs) depicting the average center of mass distribution of anions (red) and neighboring cations (green) around a fixed cation for the EMITFSI-based ILs.

3.6 Combined Distribution Functions

Combined Distribution Function (CDF) are two- or higher-dimensional histograms over certain selected scalar quantities, which are evaluated over all pairs (or n-tuples) of selected molecule in the system. **In Figure 13**, a CDF is given that relates the distance between two $[EMI]^+$ geometric ring centers (X-axis) to the angle between the ring normal vector of the one cation and the connection line between both ring centers (Y-axis). Angles close to 0◦ and 180◦ indicate that one ring is directly located on top of the other, whereas angles around 90◦ signalize that the ring is found in the ring plane of the other ring. For system A, it can be seen that the rings are around 0-30° for short distances around 200–500 pm and 180° for around 500pm which shows that the $[EMI]^+$ cation rings are almost exclusively located on top of each other. System B delivers a

similar picture. For system B, the rings are around 0° and 180° in the shorter distances around 200pm. For system C, there are more less intense peaks around 165-180° for distances 200-900pm and other less intense peaks around 0-45° for distances between 200-600pm. The situation for system D is largely different. The first large difference is the fact that the cations are only rarely found closer than 400 pm. There are very weak signals between 0-35° for distances around 500-800pm and around 180° for larger distances around 900pm. Here, the angular distribution shows that there is no preferential location of one ring relative to the other. The addition of a large amount of carbonate leads to the complete extinction of the ordering between the $[EMI]^+$ molecules.

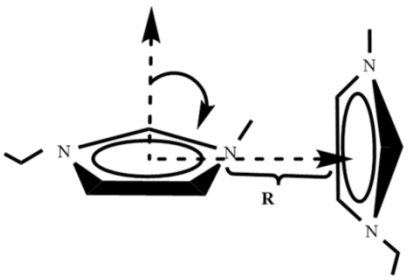

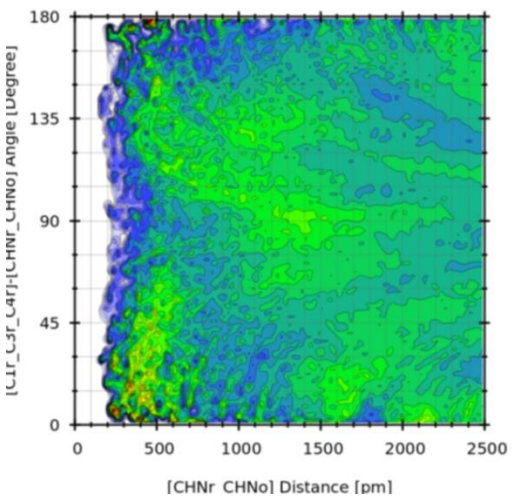

System A

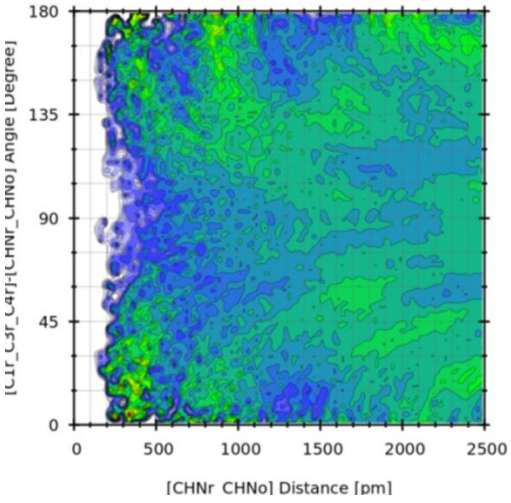

System B

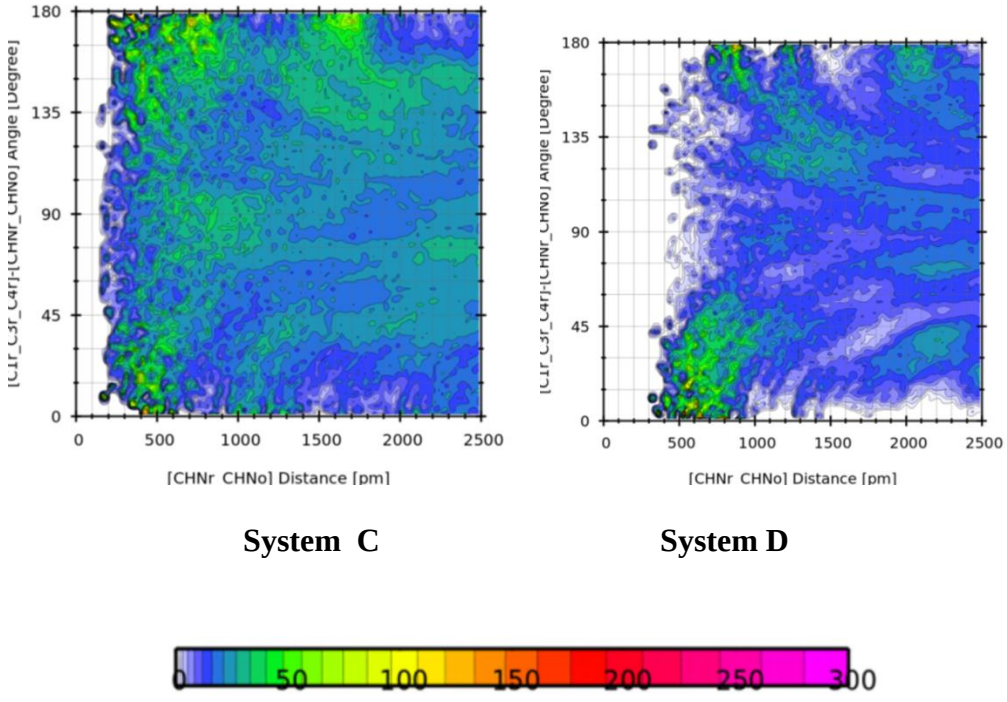

Figure 13: Combined Distribution Function showing the orientation of $[EMI]^+$ relative to other $[EMI]^+$ molecules.

In **Figure 14,** we investigate the angle between the ring planes of the $[EMI]^+$ cations in dependence on their distance. The distance axis is defined like in **Figure 13**, which was discussed above. The angular axis depicts the angle between the ring normal vectors of two $[EMI]^+$ cations. This definition is identical to the angle between the ring planes of these cations. Angles close to 0◦ and 180◦ indicate that the rings are aligned parallel to each other, whereas angles around 90◦ appear for perpendicular configurations. For system A and B, we see a clear preference of the $[EMI]^+$ rings for parallel arrangement. Intense peaks are visible around 15-30° for distances around 200-500pm and also around 150-165° for distances between 200-500pm, and very weak signals close to 180° for distances around 600-900pm. For system C, there is strong peak around 0-15° for short distances around 300-500pm. With increasing carbonate concentration (systems D), there is no preferred orientation. This implies that the rings are not only located on top of each other almost all the time, but also are mostly parallel to each other, which can be best described as the well-known ring stacking. This finding is in agreement with other AIMD simulations of imidazolium-based ILs [132]. We find that ring stacking is present in our systems A and B, which is in good agreement to recent literature on ring stacking [132].

As already observed in the previous analysis, system D shows strong differences to A and B. There are no distinct preferences for specific arrangement.

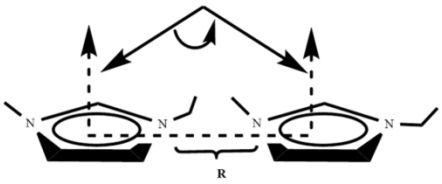

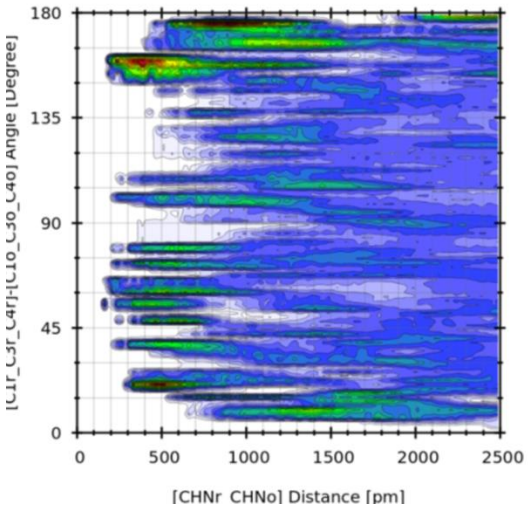

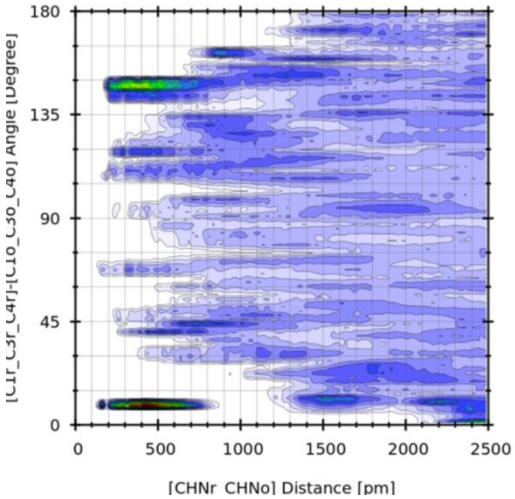

System A **System B**

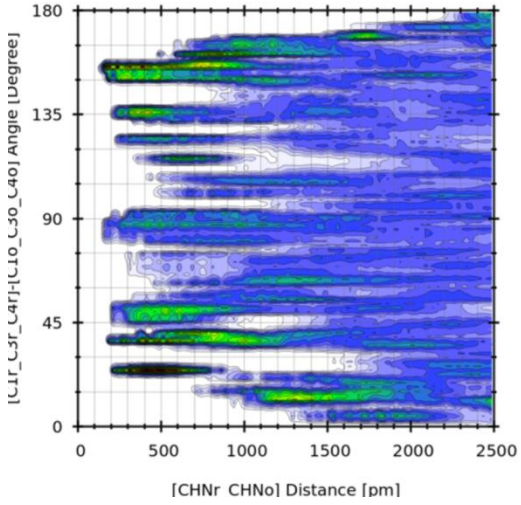

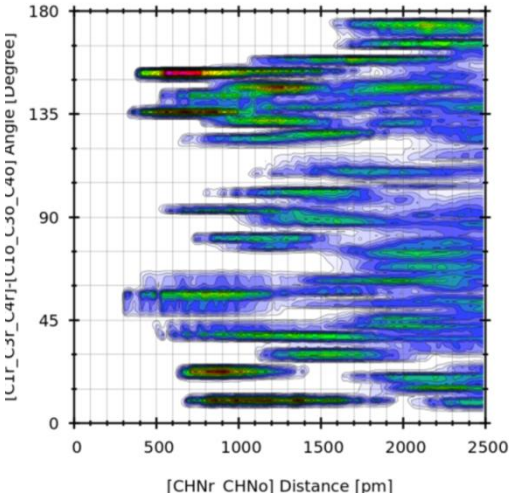

System C **System D**

Figure 14: Combined Distribution Function showing the orientation of $[EMI]^+$ relative to other $[EMI]^+$ molecules.

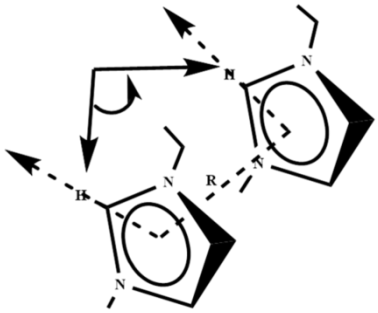

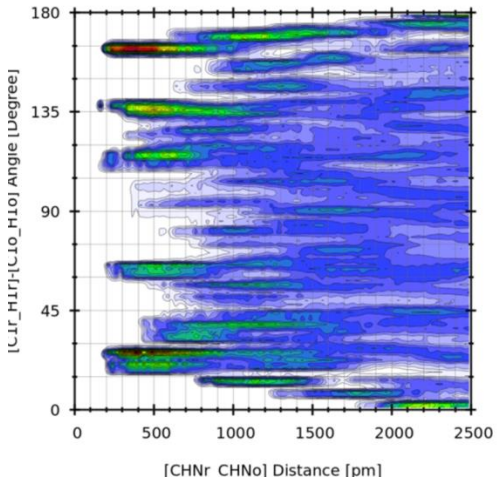

System A

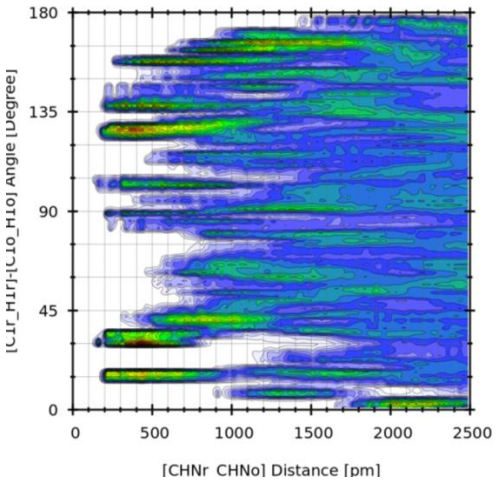

System B

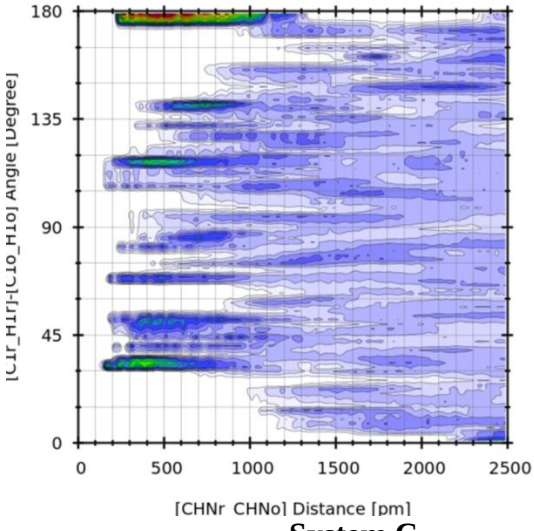

System C

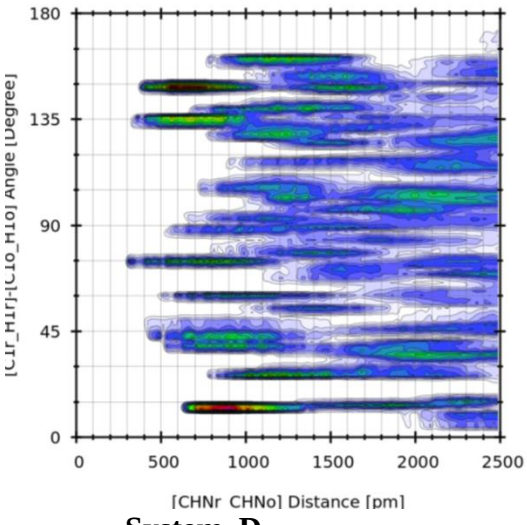

System D

Figure 15: Combined Distribution Function showing the orientation of $[EMI]^+$ relative to other $[EMI]^+$ molecules.

Within the liquid phase trajectory, the length of a certain hydrogen bond is depicted on the horizontal axis, while the hydrogen bond angle is shown on the vertical axis. In **Figure 15**, we show a CDF, in which the X axis represents the distance from the hydrogen atom H_1 of the $[EMI]^+$ cation to nitrogen atom N_1 of the $[TFSI]^-$ anion and the Y axis depicts the angle defined by the vector which goes from the H_1 atom to the C_1 atom of the cation and the vector connecting the atom H_1 and the nitrogen N_1 of the anion. A value of this angle of 180° indicates that the atoms C_1, H_1 and N_1 are aligned (the hydrogen bond would be perfectly linear). A strong peak in the region around 200 pm/105–135° and another less intense peak around 400pm/135-180° is present for the pure system A, related to the hydrogen bond between the H_1 atom of the $[EMI]^+$ cation and the N_1 atom of the $[TFSI]^-$ anion. For system B, there is a very weak signal around 400pm/150°. For systems C and D, there are no clear signals indicating that increasing the concentrations of the carbonate diminishes the hydrogen bonding between H_1 atom of the imidazolium and N_1 atom of the anion. In **Figure 16**, we show a CDF, in which the X axis represents the distance from the hydrogen atom H_1 of the $[EMI]^+$ cation to oxygen atom O_1 of the $[TFSI]^-$ anion and the Y axis depicts the angle defined by the vector which goes from the H_1 atom to the C_1 atom of the cation and the vector connecting the atom H_1 and the oxygen O_1 of the anion. A value of this angle of 180° indicates that the atoms C_1, H_1 and O_1 are aligned (the hydrogen bond would be perfectly linear). Or both system 270 and 210, a strong peak in the region around 200 pm/135° which is related to the hydrogen bond between the H1 atom of the $[EMI]^+$ cation and the O_1 atom of the $[TFSI]^-$ anion. For systems 150 and 90, there are no clear signals indicating that increasing the concentrations of the carbonate decreases the hydrogen bonding between H_1 atom of the imidazolium and O_1 atom of the anion.

In **Figures 18** and **19**, we analyze now the hydrogen bond interaction between the $[EMI]^+$ cation and the carbony oxygen of EC and DMC. A CDF is given in **Figure 18**, in which the X axis represents the distance from the hydrogen atom H_1 of the $[EMI]^+$ cation to carbonyl oxygen atom O_3 of the EC and the Y axis depicts the angle defined by the vector which goes from the H_1 atom to the C1 atom of the cation and the vector connecting the atom H1 and the oxygen O3 of EC. A value of this angle of 180° indicates that the atoms C_1, H_1 and O_3 are aligned (the hydrogen bond would be perfectly linear). In **Figure 18**, for system B, a weak signal is visible around 200pm/90-105°, 300pm/150° and another one at 1000 pm/180° indicating a very weak H_1—O_3 interaction between H1 atom of imidazolium and carbonyl oxygen of EC. For system C, a peak is clearly visible around 200pm/150°. For system D, a weak signal is visible around 700 pm/180° indicating that the interaction between the carbonyl of EC H_1 atom of $[EMI]^+$ is very minimum. In **Figure 19**, we show a CDF, in which the X axis represents the distance from the hydrogen atom H_1 of the $[EMI]^+$ cation to carbonyl oxygen atom O_3 of DMC and the Y axis depicts the angle defined by the vector which goes from the H_1 atom to the C_1 atom of the cation and the vector connecting the atom H_1 and the carbonyl oxygen O_3 of DMC. For system B, a weak signal is visible around 400pm/120° and another 400pm/60-75° indicating a very weak H_1—O_3 interaction between H_1 atom of imidazolium and carbonyl oxygen of DMC. For system C, a peak is visible around 200pm/105-120°. For system D, there is a strong peak around 300pm/150° indicating that the interaction between H1 atom of imidazolium and carbonyl oxygen of DMC increases with in increase carbonate concentration. We see that the hydrogen bond geometry between the cation and anion stays qualitatively the same for the pure ionic liquid and the system with lower carbonate content. The hydrogen bond interactions in the [EMI][TFSI] are quite weak, as even for small concentrations of IL in carbonate.

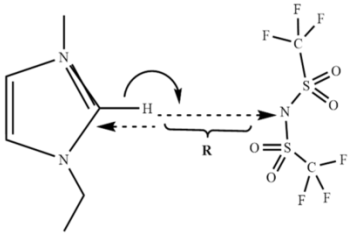

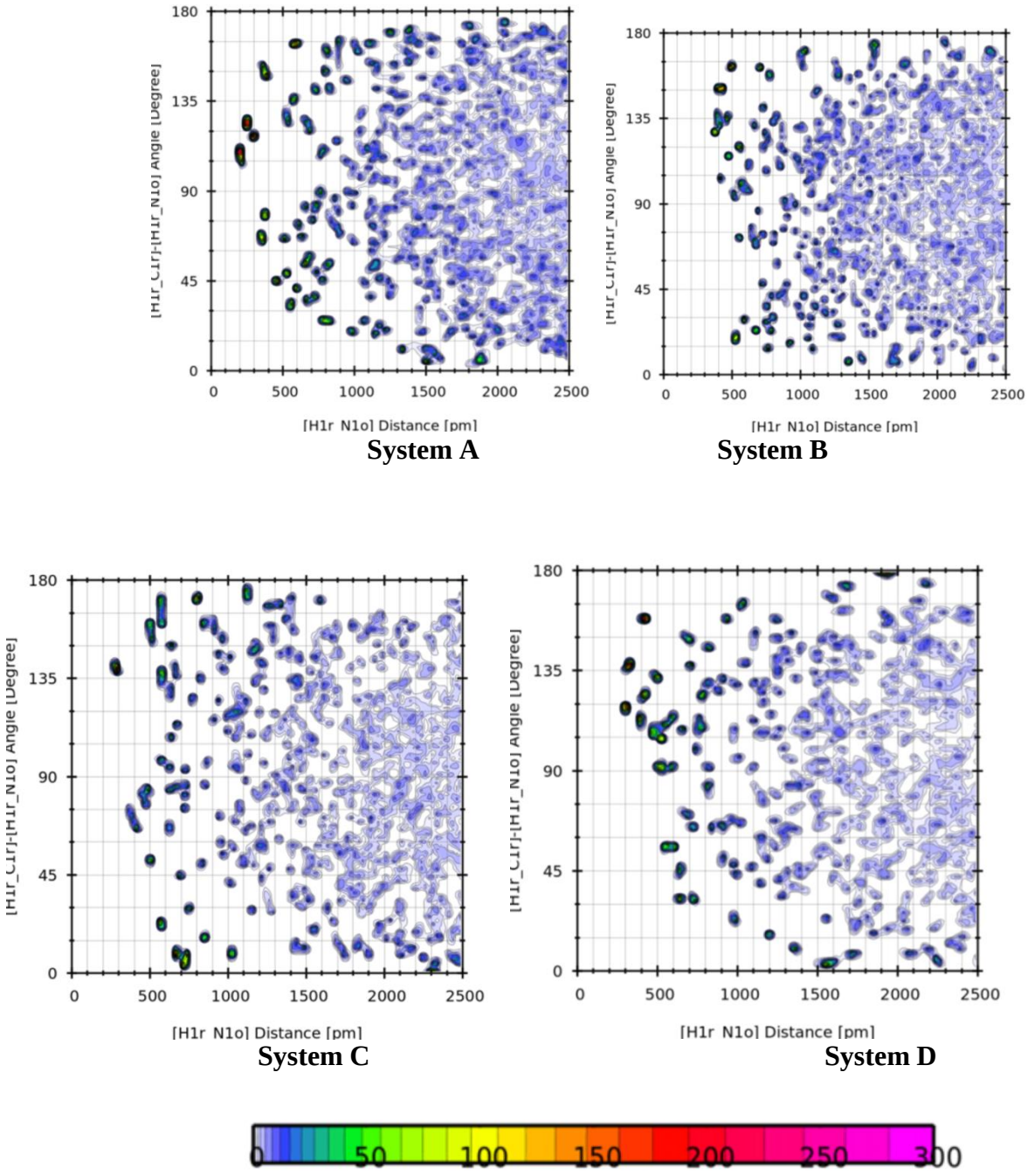

Figure 16 Combined distribution function (CDF) depicting the H1···N1 distance and the N1···H1–C1 angle in the ionic liquid [EMI][TFSI].

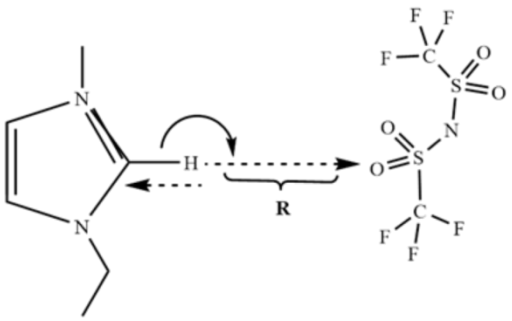

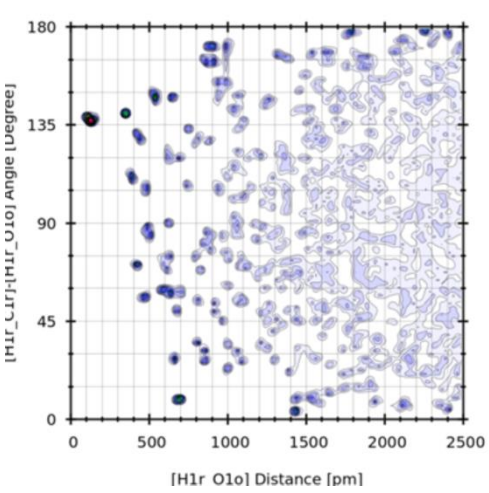

System A

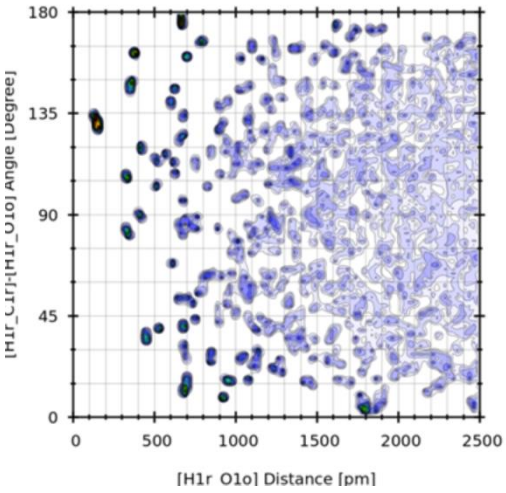

System B

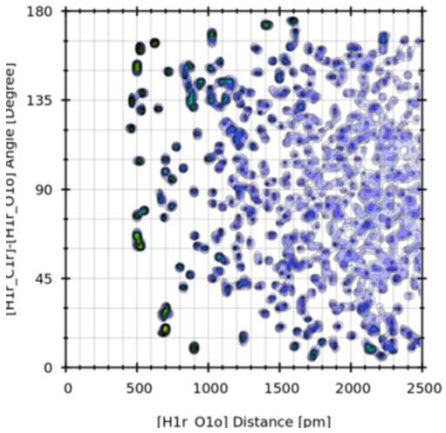

System C

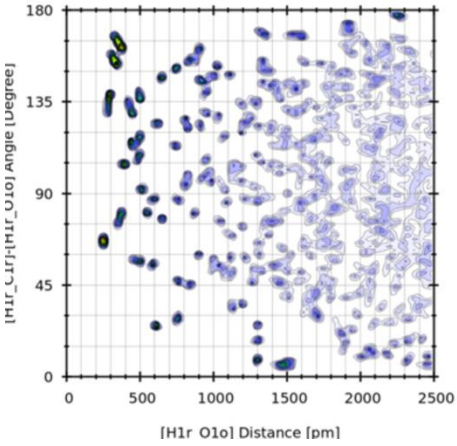

System D

Figure 17 Combined distribution function (CDF) depicting the H1···O1 distance and the O1···H1–C1 angle in the ionic liquid [EMI][TFSI].

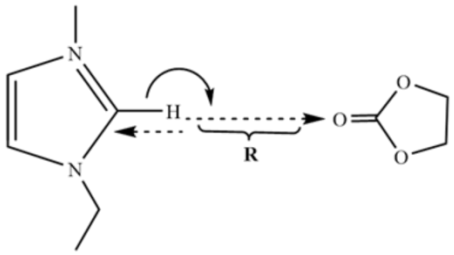

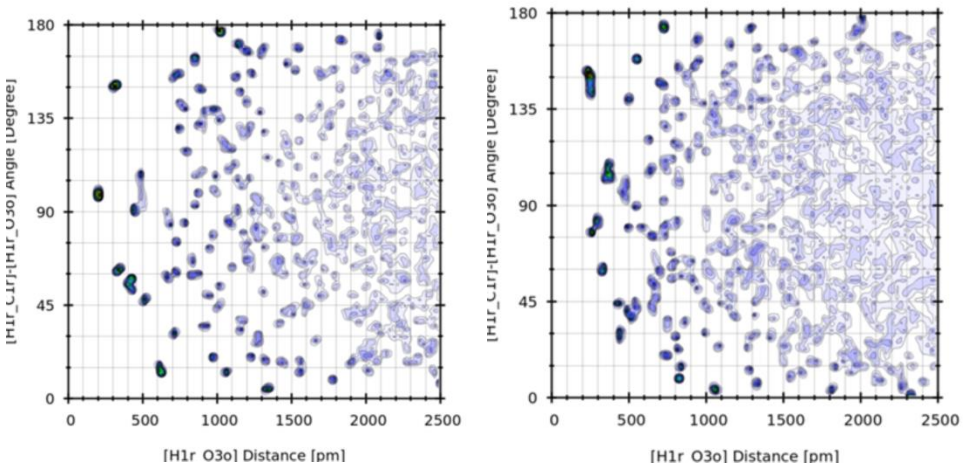

System B **System C**

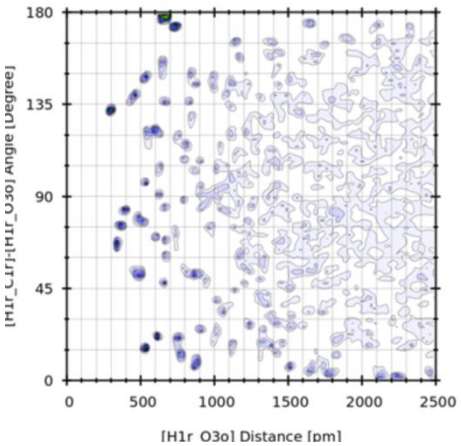

System D

Figure 18 Combined distribution function (CDF) of EC depicting the H1···O3 distance and the O3···H1–C1 angle in the ionic liquid [EMI][TFSI].

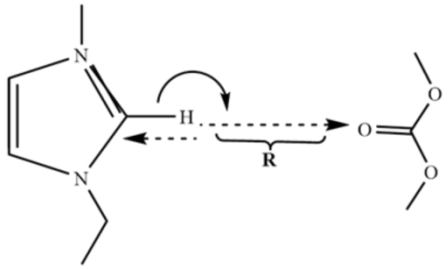

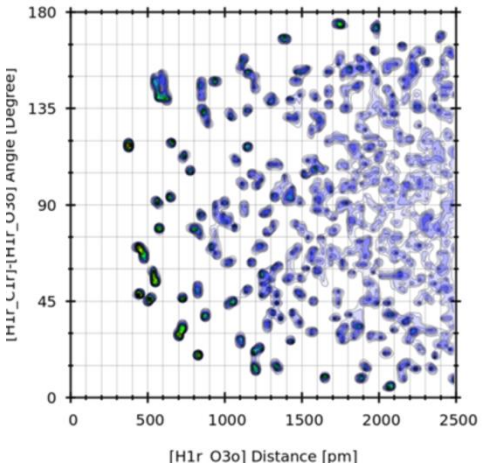

System B

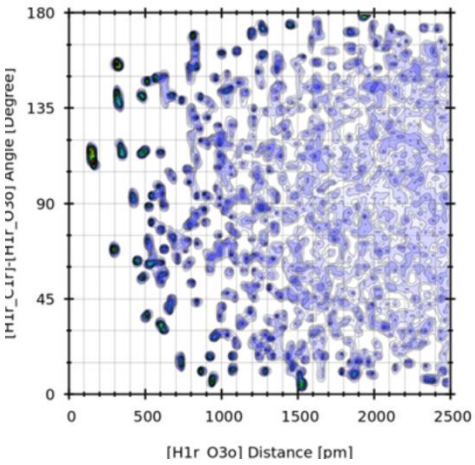

System C

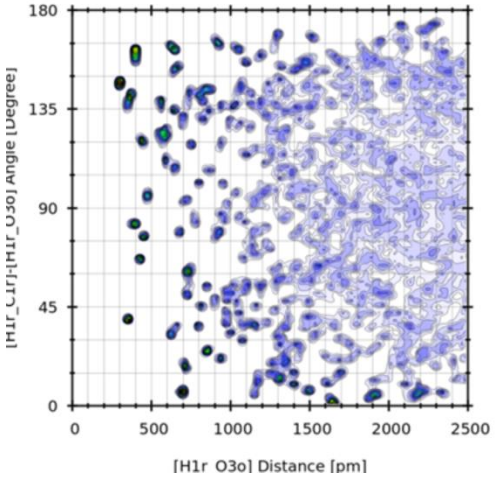

System D

Figure 19 Combined distribution function (CDF) of DMC depicting the H1···O3 distance and the O3···H1–C1 angle in the ionic liquid [EMI][TFSI].

4. Conclusion

Both density functional theory (DFT) and molecular dynamics (MD) based on classical force field were used to provide both structural and electronic insight into the multifold interactions occurring in 1-ethyl-3-methylimidazolium bis(trifluoromethylsulfonyl)imide ionic liquid in the presence of ethylene carbonate and dimethyl carbonate co-solvent mixtures which are currently being targeted for applications in next-generation Li-ion battery electrolytes. In order to give a visual understanding of the molecular interactions, the structures of cations, anions, and cation - anion ion pairs were systematically studied using DFT calculations. The nature of hydrogen bond interactions in a series of ion pair conformers have been thoroughly discussed by analyzing the interaction energies, stabilization energies and natural orbital analysis of the ion pair conformers. Multiple but weak C−H---O/N hydrogen bonds and anion donor π^*_{C-N} interactions have been observed. The doubly ionic H-bond between $[EMI]^+$ and $[TFSI]^-$ species is bifurcated, and unlike many molecular liquids, a significant variety of distinct H-bonds are formed between different types and numbers of donor and acceptor sites within the $[EMI]^+[TFSI]^-$ ion pair. The greater the number of multiple nonlinear H-bond interactions, the greater the absolute value of the interaction energy. From the NBO analysis, for [EMI][TFSI] ion pair conformers, charge transfer occurs mainly from the lone pairs of oxygen and nitrogen atom to the σ-type anti-bonding orbital of the C–H and π-type anti-bonding orbitals of N-C bonds. This is evident from the values of the stabilization energy E(2) associated with each electron delocalization from the donor to acceptor orbitals. The shorter the C–H···O and/or C–H···N bond is, the larger charge transfer, and the larger the stabilization energy E(2) associated with electron delocalization from donor to acceptor. The [EMI][TFSI] ion pair conformers tend to form multiple but bent H bonds, reducing the strength of the individual H bonds from a potential (linear) maximum. They form a major H-bond with the C^1-H^1 and a minor one with C^{alkyl}-H bonds. The relative contribution from each of these is not easily resolved via the association energy which includes the ionic as well as a combined H-bond contribution. Moreover, [EMI][TFSI] ion pairs are not symmetric

and thus cannot reach the maximum covalent contribution, which is possible only for symmetric H-bonds.

According to the radial distribution functions, for the $[EMI]^+$ cation ring centers, very weak but clear ordering can be observed. A first and a second coordination shell can be identified. The ordering between the cations is enhanced by the addition of carbonate in the mixture. The $[TFSI]^-$ anions show even a weaker ordering towards each other. Similar to the phenomenon observed for $[EMI]^+$ ring centers, The intensity (height) of the peak for the $[TFSI]^-$ anions center of mass increases by the addition of carbonate in the mixture. According to the RDFs, the addition of EC/DMC solvents into [EMI][TFSI] IL provides a more structured system than the pure [EMI][TFSI] IL system in terms of first peak heights and longer-range higher neighbor shell. The interaction between the O_1/N_1 atom of $[TFSI]^-$ and H_1 atom of $[EMI]^+$ decreases with increase in carbonate concentration. The coordination of the O_1/N_1 atom of $[TFSI]^-$ anion to H4/5 atoms of the $[EMI]^+$ cation show distinct maxima suggesting the coordination of the anion to the atom H4/5 atom of the $[EMI]^+$ cation ring. The result from RDF show that the coordination of the O_1/N_1 atom of $[TFSI]^-$ anion to the atom H_1 is much more distinct and tighter than for the other two atoms, suggesting that H1 is a stronger hydrogen bond donor than H4/5 for the pure IL system. The result from the spatial distribution functions (SDF) show that, in the pure ionic liquid, adjacent cations are almost exclusively located on top and below the $[EMI]^+$ ring, whereas the $[TFSI]^-$ anions mainly coordinate to the cation within the ring plane. The $[TFSI]^-$ anions occupy both the on top position and in plane position in the $[EMI]^+$ ring. With increasing carbonate content, however, it seems that the large amount of carbonate disturbs the original near ordering which is found in the pure ionic liquid. The results from the combined distribution function show that, in the pure ionic liquid, the orientation of the EMI^+ cations towards each other is strictly ordered. The cations are almost exclusively found on top of each other, and the ring planes of adjacent cations are parallel, which means that the rings are stacking on top of each other. This corresponds to the well-known ring stacking effect in aromatic systems, which yields in an energy gain resulting from π-π-interactions as well as London dispersion interactions.

Acknowledgments

5. References

[1] Thackeray, M. M.; Wolverton, C.; Isaacs, E. D. Energy Environ. Sci., 2012, 5, 7854−7863.

[2] Schnell, J.; Günther, T.; Knoche, T.; Vieider, C.; Köhler, L.; Just, A.; Keller, M.; Passerini, S.; Reinhart, G. J. of P. Sour., 2018, 382, 160−175.

[3] Wang, J.; Yamada, Y.; Sodeyama, K.; Chiang, C. H.; Tateyama, Y.; Yamada, A. Nat. Commun., 2016, 7, 12032.

[4] Scrosati, B.; Garche, J. Lithium batteries: Status, prospects and future. J. of P. Sour., 2010, 195, 2419−2430.

[5] Wang, Q.; Ping, P.; Zhao, X.; Chu, G.; Sun, J.; Chen, C. J. of P. Sour., 2012, 208, 210−224.

[6] Balducci, A. Topics in Current Chemistry Collections; Springer, 2017, 375, 1−27.

[7] Hanke, C. G.; Price, S. L.; Lynden-Bell, R. M. Mol. Phys., 2001, 99, 801-809.

[8] Shah, J.; Brennecke, J.; Maginn, E. Green Chem., 2002, 4, 112-118.

[9] Lynden-Bell, R. M.; Atamas, N. A.; Vasilyuk, A.; Hanke, C. G. Mol. Phys., 2002, 100, 3225-3229.

[10] Margulis, C. J.; Stern, H. A.; Berne, B. J. J. Phys. Chem. B, 2002, 106, 12017-12021.

[11] Madria, N.; Arunkumar, T. A.; Nair, N. G.; Vadapalli, A.; Huang, Y. W.; Jones, S. C.; Reddy, V. P. J. of P. Sour., 2013, 234, 277–284.

[12] Lex-Balducci, A.; Henderson, W.; Passerini, S.; Yuan, X.; Liu, H.; Zhang, J. Advanced materials and technologies. CRC Press, Boca Raton, 2011, 147–197.

[13] Guerfi, A.; Dontigny, M.; Charest, P.; Petitclerc, M.; Lagace,´ M.; Vijh, A.; Zaghib, K. J. of P. Sour., 2010, 195, 845–852.

[14] Wang, M.; Shan, Z.; Tian, J.; Yang, K.; Liu, X.; Liu, H.; Zhu, K. Electrochim. Acta., 2013, 95, 301–307.

[15] Wilken, S.; Xiong, S.; Scheers, J.; Jacobsson, P.; Johansson, P. J. of P. Sour., 2015, 275, 935–942.

[16] Ku¨hnel, S.; Bo¨ckenfeld, N.; Passerini, S.; Winter, M.; Balducci, A. Electrochim. Acta., 2011, 56, 4092–4099.

[17] Ku¨hnel, S.; Balducci, A. J. Phys. Chem. C, 2014, 118, 5742–5748.

[18] John, D.; Holbrey, W.; Matthew, R.; Robin, D. D a l t o n T r a n s., 2 0 0 4, 71, 2 2 6 7 – 2 2.

[19] Valle´e, A.; Baesner, S.; Prud'homme, J. Electrochim. Acta., 1992, 37,1579.

[20] Sakaebe, H.; Matsumoto, H. Electrochem. Commun., 2003, 5, 594.

[21] Kra¨mer, E.; Schedlbauer, T.; Hoffmann, B.; Terborg, T.; Nowak, S.; Gores, H. J.; Passerini, S.; Winter, M. J. Electrochem. Soc., 2013, 160, A356–A360.

[22] Ishikawa, M.; Sugimoto, T.; Kikuta, M.; Ishiko, E.; Kono, M. J. of P. Sour., 2006, 162, 658–662.

[23] Mauger, A.; Julien, C. M.; Paolella, A., Armand, M.; Zaghib, K. Materials Science and Engineering: R: Reports, 2018, 134, 1–21.

[24] Dahbi, M.; Ghamouss, F.; Tran-Van, F.; Lemordant, D., Anouti, M. J. of P. Sour., 2011, 196, 9743–9750.

[25] Hayes, R.; Warr, G. G.; Atkin, R. Chem. Rev., 2015, 115, 6357–6426.

[26] Araque, J. C.; Hettige, J. J.; Margulis, C. J. J. Phys. Chem. B, 2015, 119, 12727–12740.

[27] Canongia Lopes, J. N.; P´adua, A. A. H. Theor. Chem. Acc., 2012, 131, 1129.

[28] Kirchner, B.; Holl´oczki, O.; Canongia Lopes, J. N.; P´adua, A. A. H. Wiley Interdiscip. Rev. Comput. Mol. Sci., 2015, 5, 202–214.

[29] Niedermeyer, H.; Ashworth, C.; Brandt, A.; Welton, T.; Hunt, P. A. Phys. Chem. Chem. Phys., 2013, 15, 11566.

[30] Izgorodina, E. I.; Seeger, Z. L.; Scarborough, D. L. A.; Tan, S. Y. S. Chem. Rev., 2017, 117, 6696–6754.

[31] Kristyan, S.; Pulay, P. Chem. Phys. Lett., 1994, 229, 175.

[32] Hobza, P.; Sponer, J.; Reschel, T. J. J. Comput. Chem., 1995, 11, 1315.

[33] Pitonak, M.; Riley, K. E.; Neogrady, P.; Hobza, P. Phys. Chem. Chem. Phys., 2008, 9, 1636. [34] Sinnkrot, M. O.; Sherrill, C. D. J. Phys. Chem. A, 2004, 108, 10200.

[35] Cremer, D. Encyclopedia of Computational Chemistry, P. v. R. Schleyer, Ed., Wiley, New York, 1998, l.3, 1706.

[36] Tsuzuki, S.; Honda, K.; Uchimaru, T.; Mikami, M. J. Chem. Phys., 2004, 120, 647.

[37] Dion, M.; Rydberg, H.; Scroder, E.; Langreth, D. C.; Lundqvist, B. I. Phys. Rev. Lett., 2004, 92, 246401.

[38] Heβelmann, A.; Jansen, G.; Sch€utz, M. J. Chem. Phys., 2005, 122, 14103.

[39] Wu, Q.; Yang, W. J. Chem. Phys., 2002, 115, 515.

[40] Goerigk, L.; Grimme, S. J. Chem. Theory Comput., 2011, 7, 291.

[41] Juan, A.; Juan, C.; García, S.; Enrique, O.; Beljonne, D.; J. Chem. Theory Comput. 2011, 7, 2068–2077.

[42] Řezáč, J.; Hobza, P. J. Chem. Theory Comput., 2013, 9, 2151–2155.

[43] Lu, Y-X.; Zou, J-W.; Fan, J-C.; Zhao, W-N.; Jiang, Y-J.; Yu, Q-S. J. Comput. Chem., 2009, 30, N725–732.

[44] Siiskonen, A.; Priimagi, A. J. Mol. Model, 2017, 23, 50.

[45] Chai, J-D.; Head-Gordon, M. J. Chem. Phys., 2008, 128, 084106.

[46] Haskins, J. B.; Bauschlicher Jr, C. W.; Lawson, J. W. J. Phys. Chem. B, 2015, 119, 14705–14719.

[47] Ong, S. P.; Andreussi, O.; Wu, Y.; Marzari, N.; Ceder, G. Chem. Mater., 2011, 23, 2979–2986.

[48] Bauschlicher Jr, C. W.; Haskins, J. B.; Bucholz, E. W.; Lawson, J. W.; Borodin, O. J. Phys. Chem. B, 2014, 118, 10785–10794.

[49] Deetlefs, M.; Hardacre, C.; Nieuwenhuyzen, M.; Padua, A. A.; Sheppard, O.; Soper, A. K. J. Phys. Chem. B, 2006, 110, 12055–12061.

[50] Angell, C. A.; Ansari, Y.; Zhao, Z. Farad. Discuss., 2012, 154, 9–27.

[51] Liu, H.; Maginn, E. J. Chem. Phys., 2011, 135, 124507.

[52] Liu, H.; Maginn, E. Chem. Phys. Chem. 2012, 13, 1701–1707.

[53] Shah, J. K.; Brennecke, J. F.; Maginn, E. J. Green Chem., 2002, 4, 112−118.

[54] Morrow, T. I.; Maginn, E. J. J. Phys. Chem. B, 2002, 106, 12807−12813.

[55] Margulis, C. J.; Stern, H. A.; Berne, B. J. J. Phys. Chem. B, 2002, 106, 12017−12021.

[56] de Andrade, J.; Bö es, E. S.; Stassen, H. J. Phys. Chem. B, 2002, 106, 3546−3548.

[57] de Andrade, J.; Bö es, E. S.; Stassen, H. J. Phys. Chem. B, 2002, 106, 13344−13351.

[58] Hansen, J. P.; McDonalds, I. R. Theory of simple liquids, 2nd ed., Academic Press, New York, 1986.

[59] Svishchev, I. M.; Kusalik, P. G. J. Chem. Phys., 1993, 99, 3049–3058.

[60] Francesco, S.; Paola, D.; Valentina, M. Chemical Physics Letters, 2018, 691, 437-443.
[61] Frisch, M. J.; Trucks, G. W.; Schlegel, H. B.; Scuseria, G. E.; Robb, M. A.; Cheeseman, J. R.; G. Scalmani, V. Barone, B. Mennucci, G. A. Petersson, H. Nakatsuji, M. Caricato, X. Li, H. P. Hratchian, A. F. Izmaylov, J. Bloino, G. Zheng, J. L. Sonnenberg, M. Hada, M. Ehara, K. Toyota, R. Fukuda, J. Hasegawa, M. Ishida, T. Nakajima, Y. Honda, O. Kitao, H. Nakai, T. Vreven, J. A. Montgomery Jr, J. E. Peralta, F. Ogliaro, M. Bearpark, J. J. Heyd, E. Brothers, K. N. Kudin, V. N. Staroverov, R. Kobayashi, J. Normand, K. Raghavachari, A. Rendell, J. C. Burant, S. S. Iyengar, J. Tomasi, M. Cossi, N. Rega, J. M. Millam, M. Klene, J. E. Knox, J. B. Cross, V. Bakken, C. Adamo, J. Jaramillo, R. Gomperts, R. E. Stratmann, O. Yazyev, A. J. Austin, R. Cammi, C. Pomelli, J. W. Ochterski, R. L. Martin, K. Morokuma, V. G. Zakrzewski, G. A. Voth, P. Salvador, J. J. Dannenberg, S. Dapprich, A. D. Daniels, O¨. Farkas, J. B. Foresman, J. V. Ortiz, J. Cioslowski and D. J. Fox, Gaussian 09, Revision D.01, 2009.
[62] Becke, A. D. J. Chem. Phys., 1993, 98, 5648−5652.
[63] Lee, C.; Yang, W.; Parr, R. G. Phys. Rev. B, 1988, 37, 785−789.
[64] Grimme, S. J. Comput. Chem., 2006, 27, 1787−1799.
[65] Jeon, J.; Kim, H. J. J. Phys. Chem. A, 2000, 104, 9812−9815.
[66] Jeon, J.; Kim, H. J. J. Chem. Phys., 2003, 119, 8626−8635.
[67] Shim, Y.; Choi, M. Y.; Kim, H. J. J. Chem. Phys., 2005, 122, 044510.
[68] Shim, Y.; Jeong, D.; Manjari, S.; Choi, M. Y.; Kim, H. J. Acc. Chem. Res., 2007, 40, 1130−1137.
[69] Shim, Y.; Kim, H. J. J. Phys. Chem. B, 2013, 117, 11743−11752.
[70] Wang, Y.; Li, H.; Han, S. J. Chem. Phys., 123 (2005) 174501-1–174501-11.
[71] Plimpton, S. J. Comput. Phys., 1995, 117, 1–19.
[72] Jorgensen, W. L.; Maxwell, D. S., Tirado-Rives, J. J. Am. Chem. Soc., 1996, 118, 11225–11236.
[73] Doherty, B.; Zhong, X.; Gathiaka, S.; Li, B.; Acevedo, O. J. Chem. Theory Comput., 2017, 13, 6131−6145.
[74] Kaminski, R. A.; Friesner, J.; Tirado, R.; Jorgensen, W. L.; J. Phys. Chem. B, 2001, 105, 6474–6487.
[75] Lopes, J. N. C.; Padua, A. A. H., J. Phys. Chem. B, 2004, 108, 16893–16898.
[76] Jensen, K. P.; Jorgensen, W. L., J. Chem. Theory Comput., 2006, 2, 1499–1509.

[77] Martinez, L.; Andrade, R.; Birgin, E. G.; Martinez, J. M. J. Comput. Chem., 2009, 30, 2157–2164.
[78] Nose, S. J. Chem. Phys., 1984, 81, 511–519.
[79] Bussi, G.; Donadio, D.; Parrinello, M. J. Chem. Phys., 2007, 126, 014101.
[80] Humphrey, W.; Dalke, A.; Schulten, K. J. Mol. Graphics, 1996, 14, 33–38.
[81] Brehm, M.; Kirchner, B. J. Chem. Inf. Model., 2011, 51, 2007-2023.
[82] Johansson, P.; Gejji, S. P.; Tegenfeldt, J.; Lindgren, J. Electrochim. Acta., 1998, 43, 1375.
[83] Lopes, J. N. C.; Pa´dua, A. A. H, J. Phys. Chem. B, 2004, 108, 16893.
[84] Rey, I.; Lasse`gues, J.-C.; Grondin, J.; Servant, L. Electrochim. Acta., 1998, 43, 1505.
[85] Holbrey, J. D.; Reichert, W. M.; Rogers, R. D. Dalton Trans., 2004, 2267.
[86] Arnaud, R.; Benrabah, D.; Sanchez, J-Y. J. Phys. Chem., 1996, 100, 10882.
[87] Herstedt, M.; Smirnov, M.; Johansson, P.; Chami, M.; Grondin, J.; Servant, L.; Lassegues, J. C. J. Raman Spectrosc., 2005, 36, 762−770.
[88] Matsumoto, K.; Oka, T.; Nohira, T.; Hagiwara, R. Inorg. Chem., 2012, 52, 568−576.
[89] Fujii, K.; Fujimori, T; Takamuku, T.; Kanzaki, R.; Umebayashi, Y.; Ishiguro, S. J. Phys. Chem. B, 2006, 110, 8179-8183.
[90] Pérez-Jordá, J. M.; Becke, A. D. Chem. Phys. Lett., 1995, 233, 134–137.
[91] Kristyán, S.; Pulay, P. Chem. Phys. Lett., 1994, 229, 175–180.
[92] Berg, R.W..; Koel, M. CRC Press, LLC, 2009, pp. 307–354.

[93] Hamaguchi, H.; Ozawa, R. Adv. Chem. Phys., 2005, 131, 85.
[94] Katayanagi, H.; Hayashi, S.; Hamaguchi, H.; Nishikawa, K. Chem. Phys. Lett., 2004, 392, 460.
[95] Imanari, M.; Nakakoshi, M.; Seki, H.; Nishikawa, K. Chem. Phys. Lett., 2008, 459, 89.
[96] Berg, R.W. M. Koel (Ed.), CRC Press, LLC, 2009, pp. 307–354.
[97] Umebayashi, Y.; Fujimori, T. Sukizaki, T. Asada, M. Fujii, K.; Kanzaki, R.; Ishiguro, S. J. Phys. Chem. A, 2005, 109, 8976.
[98] Ozawa, R.; Hayashi, S.; Saha, S.; Kobayashi, A.; Hamaguchi, H. Chem. Lett., 2003, 32, 948.
[99] Dong, K.; Zhang, S.; Wang, D.; Yao, X.; J. Phys. Chem. A, 2006, 110, 9775-9782.

[100] Dymek, C. J., Jr.; Grossie, D. A.; Fratini, A. V.; Adams, W. W. J. Mol. Struct., 1989, 213, 25-34.

[101] Matsumoto, K.; Hagiwara, R.; Yoshida, R.; Ito, Y.; Mazej, Z.; Benkiı`, P.; Z˘ emva, B.; Tamada, O.; Yoshino, H.; Matsubara, S. Dalton Trans., 2004, 144-149.

[102] Dong, K.; Zhang, S.; Wang, D.; Yao, X. J. Phys. Chem. A, 2006, 110, 9775-9782.

[103] Umebayashi, Y.; Fujimori, T.; Sukizaki, T.; Asada, M.; Fujii, K.; Kanazaki, R.; Ishiguro, S. J. Phys. Chem. A 2005, 109, 8976−8982.

[104] Fujii, K.; Fujimori, T.; Takamuku, T.; Kanzaki, R.; Umebayashi, Y.; Ishiguro, S. J. Phys. Chem. B, 2006, 110, 8179.

[105] Lassegues, J. C.; Grondin, J.; Holomb, R.; Johansson, P. J. Raman Spectrosc. 2007, 38, 551−558.

[106] Köddermann, T.; Wertz, C.; Heintz, A.; Ludwig, R. Chem. Phys. Chem. 2006, 7, 1944−1949.

[107] Tsuzuki, S.; Tokuda, H.; Hayamizu, K.; Watanabe, M. J. Phys. Chem. B 2005, 109, 16474−16481.

[108] Dhumal, N. R.; Noack, K.; Kiefer, J.; Kim, H. J. J. Phys. Chem. A, 2014, 118, 2547−2557.

[109] Hossein, A.; Sayyed, F. T.; Nancarrow, P. J. IRAN CHEM. SOC. 2017, 14, 1281–1300.

[110] Goerigk, L.; Grimme, S. J. Chem. Theory Comput. 2011, 7, 291.

[111]. Gilli, P.; Pretto, L.; Gilli, G. J. Mol. Struct., 2007, 844–845,328–339.

[112] Jeffrey, G. A. Oxford University Press, Oxford, 1997.

[113] Patricia, A. H.; Ashworth, C. R.; Matthew, R. P. Chem. Soc. Rev.DOI: 10.1039/c4cs00278d.

[114] Deetlefs, M.; Hardacre, C. Nieuwenhuyzen, M.; Pa´dua, A. A. H.; Sheppard, O. J. Phys. Chem. B,, 2006, 110, 12055–12061.

[115] Fumino, K.; Wulf, A.; Ludwig, R. Angew. Chem., Int. Ed. 2008, 47, 8731.

[116] Deetlefs, M.; Hardacre, C.; Nieuwenhuyzen, M.; Padua, A. A.; Sheppard, O.; Soper, A. K. J. Phys. Chem. B, 2006, 110, 12055.

[117] Weber, H.; Holloczki, O.; Pensado, A. S.; Kirchner, B. J. Chem. Phys., 2013, 139, 084502.

[118] Richard, P.; Matthews, Tom, W.; Patricia, A. H. J. Phys. Chem. Chem. Phys., 2014, 16, 3238—3253

[119] Weinhold, F. J. Comput. Chem., 2012, 33, 2363–2379.

[120] Madhulata, S.; Satyen, S. Computational and Theoretical Chemistry, 2013, 1015, 27–33.

[121] Reed, A. E.; Curtiss, L .A.; Weinhold, F. Chem. Rev., 1988, 88, 899–926.

[122] Bodo, E.; Mangialardo, S.; Ramondo, F.; Ceccacci, F.; Postorino, P. J. Phys. Chem. B, 2012, 116, 13878–13888.

[123] Fumino, K.; Wulf, A.; Ludwig, R. Phys. Chem. Chem. Phys., 2009, 11, 8790–8794.

[124] Brehm, M.; Weber, H.; Pensado, A. S.; Stark, A.; Kirchner, B.; Z. Phys. Chem., 2013, 227, 177–203.

[125] Headen, T. F., Howard, C. A.; Skipper, N. T.; Wilkinson, M. A.; Bowron, D. T.; Soper, A. K. J. Am. Chem. Soc., 2010, 132, 5735.

[126] Pensado, A. S.; Brehm, M.; Thar, J.; Seitsonen, A. P.; Kirchner, B. ChemPhysChem., 2012, 13, 1845.

[127] Kohagen, M.; Brehm, M.; Thar, J.; Zhao, W.; Müller-Plathe, F.; Kirchner, B. J. Phys. Chem. B, 2011, 115, 693.

[128] Kohagen, M. Brehm, M..; Lingscheid, Y.; Giernoth, R.; Sangoro, J.; Kremer, F.; Naumov, S.; Iacob, C.; Kärger, J.; Valiullin, R.; Kirchner, B. J. Phys. Chem. B, 2011, 115, 15280.

[129] Thar, J.; Brehm, M.; Seitsonen, A. P.; Kirchner, B. J. Phys. Chem. B, 2009, 113, 15129.

[130] Brüssel, M. Brehm, M.; Kirchner, B. Phys. Chem. Chem. Phys., 2011, 13, 13617.

[131] Brüssel, M.; Brehm, M.; Kirchner, B. Phys. Chem. Chem. Phys., 2012, 14, 13204.

[132] Pensado, A. S.; Brehm, M.; Thar, J.; Seitsonen, A. P.; Kirchner, B. ChemPhysChem., 2012, 13, 1845.